J. Fluid Mech. (1997), *vol.* 345, *pp.* 1–30. Printed in the United Kingdom

The flow induced by periodic vortex rings wrapped around a columnar vortex core

By J. S. MARSHALL

Department of Mechanical Engineering and Iowa Institute of Hydraulic Research,
The University of Iowa, Iowa City, IA 52242, USA

(Received 2 April 1996 and in revised form 18 February 1997)

A study has been performed of the interaction of periodic vortex rings with a central columnar vortex, both for the case of identical vortex rings and the case of rings of alternating sign. Numerical calculations, both based on an adaptation of the Lundgren–Ashurst (1989) model for the columnar vortex dynamics and by numerical solution of the axisymmetric Navier–Stokes and Euler equations in the vorticity–velocity formulation using a viscous vorticity collocation method, are used to investigate the response of the columnar vortex to the ring-induced velocity field. In all cases, waves of variable core radius are observed to build up on the columnar vortex core due to the periodic axial straining and compression exerted by the vortex rings. For sufficiently weak vortex rings, the forcing by the rings serves primarily to set an initial value for the axial velocity, after which the columnar vortex waves oscillate approximately as free standing waves. For the case of identical rings, the columnar vortex waves exhibit a slow upstream propagation due to the nonlinear forcing. The cores of the vortex rings can also become unstable due to the straining flow induced by the other vortex rings when the ring spacing is sufficiently small. This instability causes the ring vorticity to spread out into a sheath surrounding the columnar vortex. For the case of rings of alternating sign, the wave in core radius of the columnar vortex becomes progressively narrower with time as rings of opposite sign approach each other. Strong vortex rings cause the waves on the columnar vortex to grow until they form a sharp cusp at the crest, after which an abrupt ejection of vorticity from the columnar vortex is observed. For inviscid flow with identical rings, the ejected vorticity forms a thin spike, which wraps around the rings. The thickness of this spike increases in a viscous flow as the Reynolds number is decreased. Cases have also been observed, for identical rings, where a critical point forms on the columnar vortex core due to the ring-induced flow, at which the propagation velocity of upstream waves is exactly balanced by the axial flow within the vortex core when measured in a frame translating with the vortex rings. The occurrence of this critical point leads to trapping of wave energy downstream of the critical point, which results in large-amplitude wave growth in both the direct and model simulations. In the case of rings of alternating sign, the ejected vorticity from the columnar vortex is entrained and carried off by pairs of rings of opposite sign, which move toward each other and radially outward under their self- and mutually induced velocity fields, respectively.

1. Introduction

In any three-dimensional flow in which vortex structures of very different strengths coexist in the vicinity of each other, the weaker vortices will tend to wrap around the stronger vortex structures. As this wrapping proceeds, the weaker vortices become

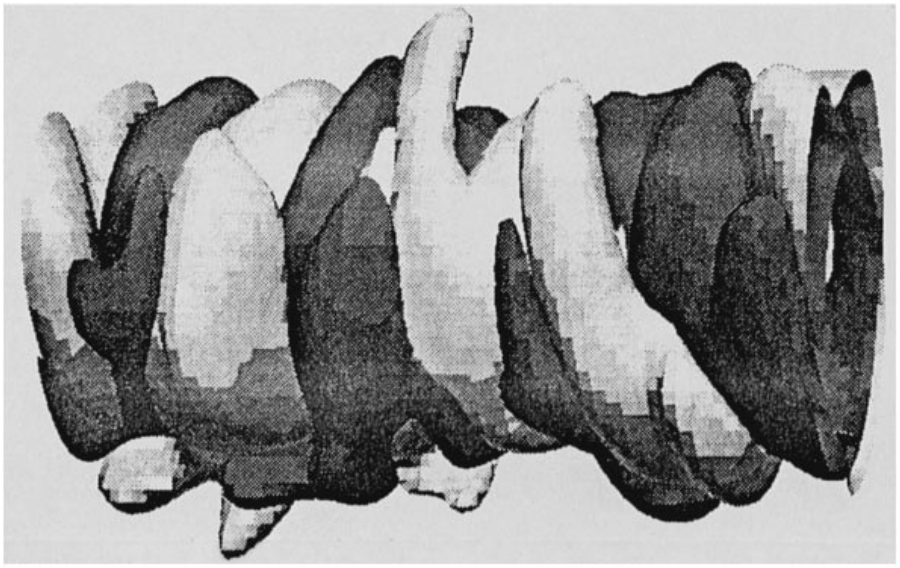

FIGURE 1. Result of a numerical simulation of the wrapping of ambient vorticity around a columnar vortex, showing the formation of wrapped ring-like vortices of opposite sign. (Reproduced with permission from Melander & Hussain 1993.)

increasing axisymmetric and may merge to create a smaller number of stronger vortices wrapped around a central (nearly columnar) vortex structure. A demonstration of the wrapping and amalgamation of weak vortices around stronger vortices is given in direct numerical simulations by Melander & Hussain (1993) for a columnar vortex immersed in an initially homogeneous turbulent flow field. Melander & Hussain observed that wrapping of the small-scale vorticity from the background turbulence about the large columnar vortex leads to an inverse cascade, which results in the formation of approximately periodic ring-like structures with alternating signs wrapped around the columnar vortex, as shown in figure 1. The existence of wrapped vortices of alternating sign around large-scale turbulent vortex structures has been confirmed experimentally, e.g. in the study by Glezer & Coles (1990) of turbulent vortex rings. Wrapping of ambient turbulence around nearly columnar vortices has also been shown to play a central role in determining the decay rate of aircraft trailing vortices in the experiments of Liu (1992) for cases with sufficiently intense atmospheric turbulence.

Wrapping of vortex structures may also occur due to three-dimensional instability of various quasi-parallel vortex systems, such as mixing layers (Bernal & Roshko 1986), vortex street wakes (Mittal & Balachandar 1995) or Taylor vortices (Sreedhar & Ragib 1994). In such flows, certain of the vortices become unstable due either to the presence of ambient shear or to interactions with other vortices (Pierrehumbert & Widnall 1982; Robinson & Saffman 1987). The unstable vortices typically elongate streamwise in the form of hairpins (with legs of alternating sign of vorticity), which interact with and sometimes wrap around other (nearly columnar) vortices. Other sources of streamwise vortex generation are discussed by Mittal & Balachandar (1995). Numerous examples of secondary vortex wrapping developing from the instability of nominally two-dimensional vortex flows are given in recent review articles by Lesieur (1996) and Sarpkaya (1996).

In a wide range of flow conditions, vortex wrapping has a controlling effect on vortex disruption in problems of three-dimensional vortex–body interaction (Kim &

Komerath 1995; Krishnamorthy & Marshall 1997), which has important applications in the area of helicopter interactional aerodynamics (Sheridan & Smith 1980). If a columnar vortex of sufficient strength is brought in the vicinity of a solid body, the vortex-induced boundary layer will separate from the body surface and wrap around the columnar vortex in the form of a series of hairpin vortices. The wrapped vorticity is observed to induce large helical and axisymmetric wave motions on the columnar vortex, sometimes even leading to disruption or bursting of the columnar vortex before it comes in contact with the solid body.

Three-dimensional wrapping of one or more (weaker) vortex structures around a (stronger) quasi-columnar vortex may involve complex flow physics, including bending and axisymmetric wave response of the quasi-columnar vortex, ejection of vorticity from the columnar vortex, impact of the head region of hairpin eddies into the columnar vortex core, and merger of the wrapped vortex structures. Some of these physical processes are fairly well understood, such as bending of vortices under their mutual interaction. Similarly, quite a lot of work has been performed on vortex merger in two dimensions (e.g. Melander, Zabusky & McWilliams 1988; Dritschel & Waugh 1992; Waugh 1992), which could readily be extended to the axisymmetric case. The current paper focuses instead on the process of vorticity ejection from the columnar vortex and the effect of axial waves of variable core area on the ejection process. While several previous papers (e.g. Melander & Hussain 1993; Mittal & Balachandar 1995) indicate the existence of deformation of the columnar vortex due to the wrapped vortices, including the formation of waves of variable core area, there seems to have been no systematic study of the columnar vortex response and vorticity ejection under the influence of these wrapped vortices.

The paper will consider an idealized flow in which the wrapped vortices are rings around a columnar vortex and the flow is constrained to be axisymmetric. The flow is required to be periodic over a fixed length L along the columar vortex axis. Cases are considered both for identical vortex rings and for vortex rings of alternating sign. One vortex ring is included in each computed period for identical vortices and two vortex rings are included in each period for rings of alternating sign. It is noted that the simulations performed in the paper suppress the leap-frogging-type instability for a row of identical rings, as predicted by Levy & Forsdyke (1927). This instability occurs for all values of the ring radius and separation distance; however, it is quite weak. For instance, consider two vortex rings with a difference ΔR in ring radius which is much smaller than the average ring radius R. It is found in the current work that the vortex ring–columnar vortex interaction occurs in a time interval over which the ring propagates a length of about one period, L. In this time, the difference in axial position between two adjacent vortex rings will change due to the leap-frog instability by an amount of approximately $(\Delta R/R)\,L$. If the ratio $\Delta R/R$ is initially small, the leap-frog instability is negligible over the time period during which the ring–columnar vortex interaction takes place.

This problem is studied computationally both via numerical simulations of the axisymmetric Navier–Stokes and Euler equations (in the vorticity–velocity formulation) using a Lagrangian vorticity collocation method (Marshall & Grant 1997) and via numerical solution of an adaptation of the Lundgren–Ashurst (1989) model for the columnar vortex dynamics under forcing from a prescribed flow induced by periodic vortex rings. The vorticity collocation method for axisymmetric swirling flows uses ring-shaped overlapping vorticity elements, with Gaussian vorticity distribution in the element cross-sections. Additional blob-like elements are used to resolve the axial vorticity along the symmetry axis. The induced velocity field is obtained by the Biot–

Savart integration over the vorticity field, where the element amplitudes are obtained using the iterative fitting procedure of Marshall & Grant (1996).

The problem is set up in section 2, followed by a brief description of the vorticity collocation method of Marshall and Grant (1997). An adaptation of the Lundgren–Ashurst model for the columnar vortex dynamics under the ring-induced velocity field is described in §3. Results of a sample numerical solution are presented in §4 for free-standing waves on a columnar vortex core, and predictions of the numerical method of §2 are compared with an analytical solution from the approximate model of §3. The analytical and computational methods described in §§2 and 3 are used to examine the ring–columnar vortex interaction for the case of identical rings in §5 and for the case of rings of alternating sign in §6. Conclusions are given in §7.

2. Problem set-up and numerical solution method

We consider the evolution of an axisymmetric swirling flow with periodic vortex rings enclosing a columnar vortex. The flow is initialized with rings of circular cross-section, having core radius σ_R, strength Γ_R and centroid radial location R in a cylindrical polar coordinate system. The columnar vortex initially has a uniform core radius σ_C and a strength Γ_C. The vorticity within the rings initially lies in the azimuthal direction and is proportional to the radial location r, as would be the case for members of the family of vortex rings considered by Norbury (1973). The vorticity within the columnar vortex is initially oriented in the axial direction and is uniform with r. The flow is assumed to remain periodic over a length L along the columnar vortex axis for all time.

The transport equations for the components $(\omega_r, \omega_\theta, \omega_z)$ of vorticity in cylindrical polar coordinates in an incompressible axisymmetric flow are

$$\frac{\mathrm{d}\omega_r}{\mathrm{d}t} = \omega_r \frac{\partial u}{\partial r} + \omega_z \frac{\partial u}{\partial z} + \nu \left[\nabla^2 \omega_r - \frac{\omega_r}{r^2} \right], \tag{1a}$$

$$\frac{\mathrm{d}\omega_\theta}{\mathrm{d}t} = \frac{\omega_\theta u}{r} - \frac{2\omega_r v}{r} + \nu \left[\nabla^2 \omega_\theta - \frac{\omega_\theta}{r^2} \right], \tag{1b}$$

$$\frac{\mathrm{d}\omega_z}{\mathrm{d}t} = \omega_r \frac{\partial w}{\partial r} + \omega_z \frac{\partial w}{\partial z} + \nu \nabla^2 \omega_z, \tag{1c}$$

where $\mathrm{d}/\mathrm{d}t$ is the material derivative, (u, v, w) are the (r, θ, z) components of the velocity vector $\boldsymbol{u}$, ∇^2 is the Laplacian operator in cylindrical polar coordinates and ν is the kinematic viscosity. The vorticity components are subject to the radial boundary conditions $\omega_r = \omega_\theta = 0$ and $\partial\omega_z/\partial r = 0$ on the symmetry axis $r = 0$, $\boldsymbol{\omega} \to 0$ faster than r^{-4} as $r \to \infty$ and periodic boundary conditions in the axial direction. The flow is initialized with $\omega_z = \Gamma_C/\pi\sigma_C^2$ and $\omega_r = \omega_\theta = 0$ within the columnar vortex and $\omega_\theta = Ar$ and $\omega_r = \omega_z = 0$ within the vortex rings. The constant A is set such that the circulation of each ring is Γ_R for the case of identical rings and $\pm\Gamma_R$ for the case of rings of alternating signs.

The velocity field is obtained as the curl of the vector potential $\boldsymbol{\beta} = -\nabla^2\boldsymbol{\omega}$, such that

$$u = -\frac{\partial \beta_\theta}{\partial z}, \quad v = \frac{\partial \beta_r}{\partial z} - \frac{\partial \beta_z}{\partial r}, \quad w = \frac{1}{r}\frac{\partial}{\partial r}(r\beta_\theta). \tag{2}$$

The Green's function solution for the components of $\boldsymbol{\beta}$ is

$$\beta_r(r,\theta,z,t) = \frac{1}{4\pi}\int_V \frac{\omega'_r\cos(\theta-\theta')+\omega'_\theta\sin(\theta-\theta')}{s}\,\mathrm{d}v', \tag{3a}$$

$$\beta_\theta(r,\theta,z,t) = \frac{1}{4\pi}\int_V \frac{\omega'_\theta\cos(\theta-\theta')-\omega'_r\sin(\theta-\theta')}{s}\,\mathrm{d}v', \tag{3b}$$

$$\beta_z(r,\theta,z,t) = \frac{1}{4\pi}\int_V \frac{\omega'_z}{s}\,\mathrm{d}v', \tag{3c}$$

where $s = [(z-z')^2+r^2+(r')^2-2rr'\cos(\theta-\theta')]^{1/2}$ and $\mathrm{d}v' = r'\,\mathrm{d}r'\,\mathrm{d}\theta'\,\mathrm{d}z'$.

The ring–columnar vortex interaction is studied by numerical solution of the system (1)–(3) using the Lagrangian vorticity collocation method of Marshall & Grant (1997) for axisymmetric swirling flows. In this method, the vorticity is evolved on a set of N control points in the (r,z)-plane, which for inviscid flows are advected by the local fluid velocity. For viscous flows, the control points are advected with an additional 'diffusion velocity' in order to account for the effect of diffusion in spreading the vorticity support. Given the vorticity values at the control points, the induced velocity is obtained in the numerical computations by interpolating the vorticity field using a representation consisting of ring-like elements for points sufficiently far removed from the symmetry axis and three-dimensional blob-like elements for points lying on the symmetry axis. This representation may be expressed symbolically as

$$\boldsymbol{\omega}(\boldsymbol{x},t) = \sum_{n=1}^{N} \boldsymbol{G}_n(t) f_n(\boldsymbol{x}-\boldsymbol{x}_n). \tag{4}$$

The element centroids $\boldsymbol{x}_n$ are advected both by the velocity induced by other vorticity elements and the element self-induced velocity. The element *amplitude* $\boldsymbol{G}_n$ represents the integral of vorticity associated with the control point over the element cross-section. The *weighting function* $f_n(\boldsymbol{x}-\boldsymbol{x}_n)$ specifies the distribution of vorticity within the element core and is normalized such that

$$\int_A f_n(\boldsymbol{x}-\boldsymbol{x}_n)\, r\,\mathrm{d}r\,\mathrm{d}z = r_n \tag{5a}$$

for the ring-like elements and

$$\int_A f_n(\boldsymbol{x}-\boldsymbol{x}_n)\, r\,\mathrm{d}r\,\mathrm{d}z = R_E \tag{5b}$$

for the blob-like elements. Here A denotes the (r,z)-plane, r_n is the radial position of control point n and R_E is the 'exclusion distance' of ring-like elements from the symmetry axis, which is usually taken to be on the order of the radius of the ring-like elements. In the present computations, both ring-like and blob-like elements are assumed to have Gaussian vorticity distribution over a cross-section, so we can write

$$f_n(\boldsymbol{x}-\boldsymbol{x}_n) = C_n \exp\left[-\frac{(z-z_n)^2+(r-r_n)^2}{\delta_n^2}\right], \tag{6}$$

where δ_n is the element radius. The normalization constant is obtained as

$$C_n = \frac{2r_n}{\pi^{1/2}\delta_n^3 + 2\pi r_n\,\delta_n^2} \tag{7a}$$

for ring-like elements and as

$$C_n = \frac{2R_E}{\pi^{1/2}\delta_n^3} \tag{7b}$$

for blob-like elements.

Substituting (4) into the integrals (3), and using the method of Laplace integrals to approximate the integrals for small values of δ_n/r_n, the induced velocity from the nth ring-like element at a point (r, z) is obtained from (2) as

$$u_n(r,\theta,z,t) = \frac{(z-z_n)\,G_\theta k_n\,\xi_n}{4\pi(r_n\,r^3)^{1/2}\,k_n'^2}[(1-\tfrac{1}{2}k_n^2)\,E(k_n)-k_n'^2\,K(k_n)], \tag{8a}$$

$$\begin{aligned} v_n(r,\theta,z,t) = &-\frac{(z-z_n)\,G_r k_n\,\xi_n}{4\pi(r_n\,r^3)^{1/2}\,k_n'^2}[(1-\tfrac{1}{2}k_n^2)\,E(k_n)-k_n'^2\,K(k_n)] \\ &-\frac{r_n\,G_z k_n\,\xi_n}{4\pi(r_n\,r^3)^{1/2}\,k_n'^2}\left[-k_n'^2\,K(k_n)+\left\{1-\tfrac{1}{2}k_n^2\left(1+\frac{r}{r_n}\right)\right\}E(k_n)\right], \end{aligned} \tag{8b}$$

$$w_n(r,\theta,z,t) = \frac{k_n\,G_\theta\,\xi_n}{8\pi(r_n\,r^3)^{1/2}\,k_n'^2}[(r+r_n)\,k_n^2\,E(k_n)-2r\{E(k_n)-k_n'^2\,K(k_n)\}], \tag{8c}$$

where (G_r, G_θ, G_z) are the components of $\boldsymbol{G}_n$ and $K(\cdot)$ and $E(\cdot)$ are complete elliptic integrals. The parameters k_n and k_n' are defined by

$$k_n^2 \equiv \frac{4rr_n}{(z-z_n)^2+(r+r_n)^2}, \quad k_n'^2 \equiv 1-k_n^2, \tag{9}$$

and ξ_n is a regularization function given by

$$\xi_n = 1-\exp\left[-\frac{(z-z_n)^2+(r-r_n)^2}{\delta_n^2}\right]. \tag{10}$$

This regularization is found to perform well in validation calculations even in cases where $\delta_n/r_n = O(1)$.

Similarly, the velocity induced by the nth blob-like element at a point $\boldsymbol{x}$ is given by

$$\boldsymbol{u}_n(\boldsymbol{x},t) = \frac{P(\frac{3}{2},|\boldsymbol{x}-\boldsymbol{x}_n|^2/\delta_n^2)\,\delta_n^3\,\pi^{1/2}C_n}{4|\boldsymbol{x}-\boldsymbol{x}_n|^3}\,\boldsymbol{G}_n\times(\boldsymbol{x}-\boldsymbol{x}_n), \tag{11}$$

where $P(a, z)$ is the incomplete gamma function, with limits $P = 0$ at $z = 0$ and $P = 1$ as $z \to \infty$, and C_n is the normalization constant given by (7b). When $a = 3/2$ and $z = x^2$, for some real variable x, a convenient expression for $P(3/2, x^2)$ is given in terms of the error function $\mathrm{erf}\,(x)$ as (Abramowitz & Stegun 1965)

$$P(\tfrac{3}{2},x^2) = \mathrm{erf}\,(x)-2x\,\mathrm{e}^{-x^2}/\pi^{1/2}. \tag{12}$$

The element amplitudes are obtained by fitting the vorticity representation (4) to the known vorticity values at the control points at every time step, using the approximate iteration procedure of Marshall & Grant (1996):

$$\boldsymbol{\omega}(\boldsymbol{x}_m,t) = \boldsymbol{G}_m^{(q+1)}\sum_{n\in Q(m)}W_{mn}+\sum_{n\in P(m)}W_{mn}\,\boldsymbol{G}_n^{(q)}, \tag{13}$$

where q is an iteration index, $Q(m)$ is a set of control points very close to control point m and $P(m)$ is the complement of $Q(m)$. The procedure (13) converges very quickly, and the number of iterations required for convergence seems to be independent of the number of control points. This iterative procedure can be used to simultaneously obtain the amplitudes of both the off-centre ring-like elements and the centre blob-like elements.

The self-induced velocity, $\boldsymbol{w}_n$, of a ring-like element with Gaussian vorticity variation in the element cross-section is given by Saffman (1970) as

$$\boldsymbol{w}_n = \frac{G_\theta}{4\pi r_n}[\ln(8r_n/\delta_n) - 0.558]\,\hat{\boldsymbol{z}}. \tag{14}$$

The blob-like elements, of course, have no self-induced velocity. The importance of the element self-induced velocity, in comparison with the velocity induced by all of the other vorticity elements, depends on the resolution of the flow field. For instance, if the core of an isolated vortex ring is discretized by N ring-like elements, the ratio of the self-induced propagation velocity of an element to the propagation velocity of the ring as a whole is of order $1/N$. The effect of the element self-induced velocity was examined in numerical calculations by Strickland & Amos (1992) and Acton (1980), both of whom concluded that for a well-resolved vorticity field the element self-induced velocity is either very small or negligible.

Viscous diffusion is accounted for in this method using a three-dimensional formulation of the diffusion velocity method of Ogami & Akamatsu (1991), and corrected by Kempka & Strickland (1993) for two-dimensional flows, to adaptively spread the vorticity support. Derivatives over the set of control points are computed using the moving least-square method introduced by Marshall & Grant (1997), in which a quadratic function is fit locally to the control points closest to the point at which the derivatives are desired using a least-squares formulation. This differentiation method maintains high accuracy even for control points which are very irregularly spaced. An explicit second-order predictor–corrector method is used to advance the solution in time, subject to a viscous stability restriction of the form

$$\Delta t \leqslant l^2 s/(2\nu), \tag{15}$$

where l is the minimum distance between any two control points, ν is the kinematic viscosity and s is an adjustable constant. The diffusion scheme is stable provided that s is less than about 7; however, in the computations reported in the present paper we set $s = 0.5$. Details of the viscous diffusion method and validation calculations can be found in Marshall & Grant (1997).

3. An approximate vortex interaction model

A plot of the radial variation of the axial velocity induced by the periodic vortex rings, with infinitesimally small core radius, is given in figure 2 for a case with $L/R = 2$ and for different values of z/L. The induced axial velocity profile is observed to be fairly uniform with r for r/R less than about 0.5 (varying by at most 15%). This observation suggests that the dynamics of the columnar vortex, for cases where $(R-\sigma_R)/\sigma_C$ is sufficiently large, may be approximated using a model in which the rings induce a prescribed axial flow on the columnar vortex which is uniform in the radial direction. The ring-induced axial velocity may be approximated by assuming that the ring core radius is small compared to the radial position of the ring centroid and by evaluating the ring-induced axial velocity on the symmetry axis. The axial velocity at an axial location z induced on the columnar vortex from periodic vortex rings is then given by

$$w_R(z,t) = \frac{1}{2}\sum_{n=-\infty}^{\infty} \frac{\Gamma_{R,n} R^2}{[(z-Z_n)^2 + R^2]^{3/2}}, \tag{16}$$

where Z_n is the axial position and $\Gamma_{R,n}$ the strength of ring n.

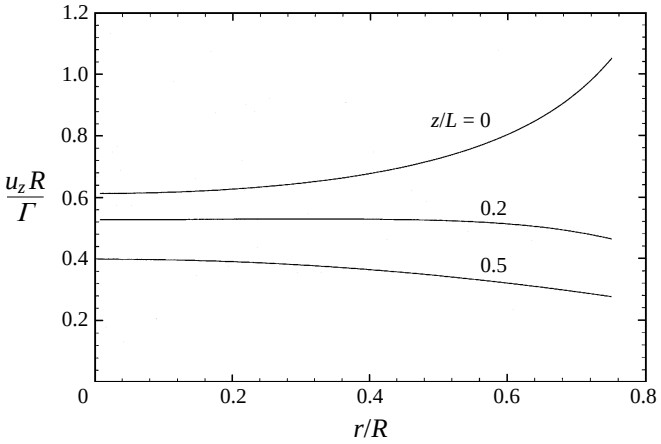

FIGURE 2. Axial velocity profiles induced by an array of periodic identical rings with $L/R = 2$, at axial sections $z/L = 0$, 0.2 and 0.5.

For the case of identical rings (such that $\Gamma_{R,n} = \Gamma_R$ for all n), the system as a whole translates in the axial direction due to both the self-induced velocity, W_s, of the rings and the propagation velocity, W_0, of each ring due to the induced velocity of all the other rings. In a frame translating with the rings, the axial velocity induced by the rings on the columnar vortex, $w_R - W_0$, is independent of time for identical rings. For the case of rings of alternating sign (such that $\Gamma_{R,n} = (-1)^n \Gamma_R$), the values of W_s and W_0 are equal and opposite for rings of opposite sign, so that the system as a whole is fixed but the axial and radial locations of the rings change with time according to

$$\frac{\mathrm{d}Z_n}{\mathrm{d}t} = \pm(W_{0,n} + W_{s,n}), \quad \frac{\mathrm{d}R}{\mathrm{d}t} = U_0, \tag{17}$$

where U_0 is the radial velocity induced on each ring by the other rings. In this case, the ring-induced axial velocity w_R is a function of both z and t.

The self-induced propagation velocity of ring n, $W_{s,n}$, is given approximately by (Kelvin 1867)

$$W_{s,n} = \frac{\Gamma_{R,n}}{4\pi R}[\ln(8R/\sigma_R) - 0.25]. \tag{18}$$

The axial and radial velocity components of the nth ring induced by the other rings are given by

$$W_{0,n} = \frac{1}{4\pi R} \sum_{m=-\infty}^{\infty} \Gamma_{R,m} k_{nm}[K(k_{nm}) - E(k_{nm})], \tag{19}$$

$$U_0 = \frac{1}{4\pi R^2} \sum_{m=-\infty}^{\infty} \frac{(Z_n - Z_m)\Gamma_m k_{nm}}{k'^2_{nm}}[(1 - \tfrac{1}{2}k^2_{nm})E(k_{nm}) - k'^2_{nm} K(k_{nm})], \tag{20}$$

where k_{nm} is defined by

$$k^2_{nm} = \frac{4R^2}{(Z_n - Z_m)^2 + 4R^2} \tag{21}$$

and $k'^2_{nm} \equiv 1 - k^2_{nm}$. The radial velocity U_0 is the same for all n for the two cases considered in this paper.

The columnar vortex dynamics can be further simplified by assuming that the axial components of vorticity and velocity within the columnar vortex have a constant prescribed profile in the radial direction, such that these quantities have the same functional dependence on r/σ for all z and t, where $\sigma(z,t)$ denotes the core radius of the columnar vortex for any given z and t. For simplicity, we will henceforth assume that both the axial vorticity and axial velocity are uniform over the cross-section of the columnar vortex core, and that the radial and azimuthal velocity components vary linearly with r. Letting $w(z,t)$ denote the vortex axial velocity relative to a reference frame translating with the mean position of the ring centroids, the centre vortex evolution can be described by a set of two model equations for σ and w. These equations have been previously derived (without forcing by the vortex rings) using a variety of different approaches by Lundgren & Ashurst (1989), Marshall (1991) and Leonard (1994), all of which yield essentially the same results for long weakly nonlinear wave motions. In its simplest form (as given by Lundgren & Ashurst 1989), the evolution of the columnar vortex is governed by volume conservation of the core fluid, which requires that

$$\frac{\mathrm{d}\sigma}{\mathrm{d}t}+\frac{\sigma}{2}\frac{\partial w}{\partial z}=0, \tag{22}$$

and by axial momentum conservation, which in the presence of the vortex rings requires that

$$\pi\sigma^2\frac{\mathrm{d}w}{\mathrm{d}t}=-\frac{\Gamma_C^2}{4\pi\sigma}\frac{\partial\sigma}{\partial z}+\pi\sigma^2 w_R\frac{\partial w_R}{\partial z}, \tag{23}$$

where

$$\frac{\mathrm{d}f}{\mathrm{d}t}\equiv\frac{\partial f}{\partial t}+w\frac{\partial f}{\partial z} \tag{24}$$

is the material derivative. Equation (23) represents a balance between the rate of change of axial momentum within the columnar vortex core and an axial force due to the pressure gradient along the vortex axis which is induced by variation of the core radius and the flow induced by the vortex rings.

Equations (22) and (23) admit solutions for small-amplitude waves, for which the dispersion relationship yields the phase velocity c of the waves as

$$c=\Gamma_C/(\sqrt{8}\,\pi\sigma_C). \tag{25}$$

For vortex flows with axial velocity greater than the phase velocity c, upstream wave propagation is not possible and the flow is said to be 'supercritical'. Similarly, vortex flows with axial velocity less than the phase velocity are said to be 'subcritical'.

Equations (22) and (23) form a hyperbolic first-order system, which can be written in the conservation form

$$\frac{\partial(\sigma^2)}{\partial t}+\frac{\partial}{\partial z}(\sigma^2 w)=0, \tag{26a}$$

$$\frac{\partial w}{\partial t}+\frac{\partial}{\partial z}\left(\frac{w^2}{2}-\frac{\Gamma_C^2}{8\pi^2\sigma^2}\right)=\frac{\partial w_R}{\partial t}+w_R\frac{\partial w_R}{\partial z}. \tag{26b}$$

Numerical solution of (26) is performed using the two-step MacCormack method, in which axial derivatives are evaluated using a forward difference on the predictor step and a backward difference on the corrector step (Peyret & Taylor 1990). The boundary

conditions in the z-direction assume that the flow is periodic with wavelength L, and the initial conditions are chosen as $\sigma(z,0) = \sigma_C$ and $w(z,0) = w_R(z,0) - W_S - W_0$ (for identical rings) or $w(z,0) = w_R(z,0)$ (for rings of alternating sign), where w_R is given by (16).

4. Sample calculation for standing waves on a vortex core

The vorticity collocation method described in §2 is used in the current section to compute small-amplitude standing waves on a vortex core, and the result is compared to an analytical solution obtained from the model equations (22) and (23) of §3 with $w_R = 0$. We consider small-amplitude standing waves on a columnar vortex core for which the core radius varies as

$$\sigma(z,t) = \sigma_C + A\cos(\alpha t)\cos(kz), \tag{27}$$

where $k = 2\pi/L$ is the wavenumber and α is the oscillation frequency. The solution of the system (22) and (23), after linearizing for small A/σ_C, yields an expression for the wave period $p = 2\pi/\alpha$ as

$$p = 4\sqrt{2}\,\pi^2\sigma_C/(k\Gamma_C). \tag{28}$$

Calculations using the vorticity collocation method were performed for the evolution of a columnar vortex which was initially perturbed by a variation in core radius in the form of a cosine wave, with wave amplitude of 10% of the mean core radius, and wavelength equal to four times the mean core radius. The core is discretized by 1619 ring-like vorticity elements for off-centre points and 81 blob-like elements are placed along the symmetry axis. The axial component of the initial vorticity field is specified to be independent of r and to vary with z in such a way that the circulation remains constant along the vortex axis. The radial component of the initial vorticity is specified to vary linearly with r, such that the vorticity vector is parallel to the core boundary for the outermost points on the vortex core. One period on each side of the computed section is used in the velocity calculation.

The computations using the vorticity collocation method yield a standing wave on the vortex core which oscillates nearly periodically in time. The radial and axial velocity components within the standing wave are shown in figures 3(*a*) and 3(*b*), using an arrow attached to each control point, for times separated by about one-half of the oscillation period. In these figures, the dimensionless time is defined as $t^* \equiv t\Gamma_C/\sigma_C^2$. The axial motion within the standing wave is generated by oscillating azimuthal vorticity, which forms when the predominantly axial vorticity component is tilted in the azimuthal direction by an axial gradient in the swirl velocity, which arises from variation of the core radius. The core radius variation also causes a radial tilting of the vorticity vector which, in the presence of the ambient radial gradient of the swirl rate near the edge of the vortex core, leads to additional accumulation of the azimuthal vorticity. In the resulting wave motion, the azimuthal vorticity magnitude attains a minimum value when the slope of the core boundary is greatest, and vice versa. A contour plot of the azimuthal vorticity field, obtained by interpolating the vorticity onto a 81×201 grid in the (r,z)-plane using the representation (4), is shown in figure 4 at the same two times as used in the velocity vector plots of figure 3. The reversal of the azimuthal vorticity which occurs during the wave oscillation is clearly evident in this plot.

The average value of the element radius during the computations was found to be $0.12\sigma_C$, so that the effective core radius of the columnar vortex is approximately

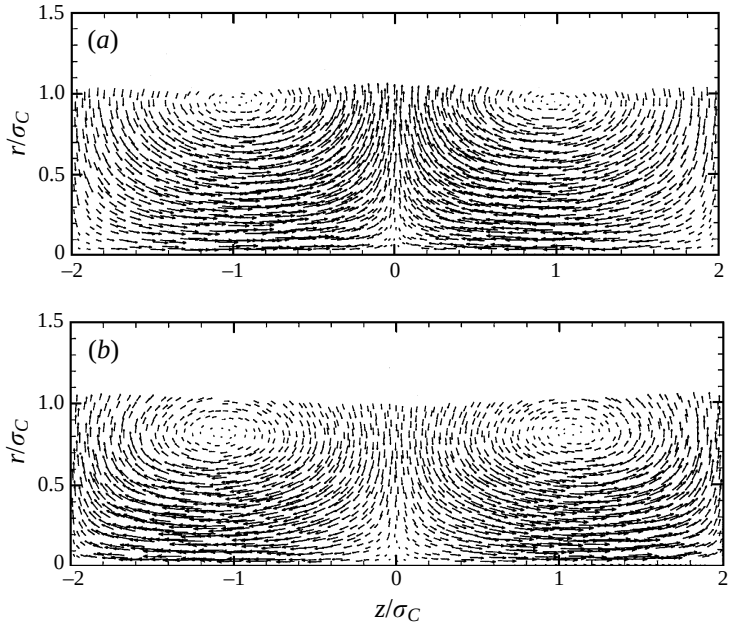

FIGURE 3. Velocity vectors in the (r, z)-plane within a standing vortex wave with initial amplitude of 10% of the mean core radius, at dimensionless times (*a*) $t^* = 11.4$ and (*b*) $t^* = 35.4$. The wave oscillates nearly periodically in time with a dimensionless period of 42.3.

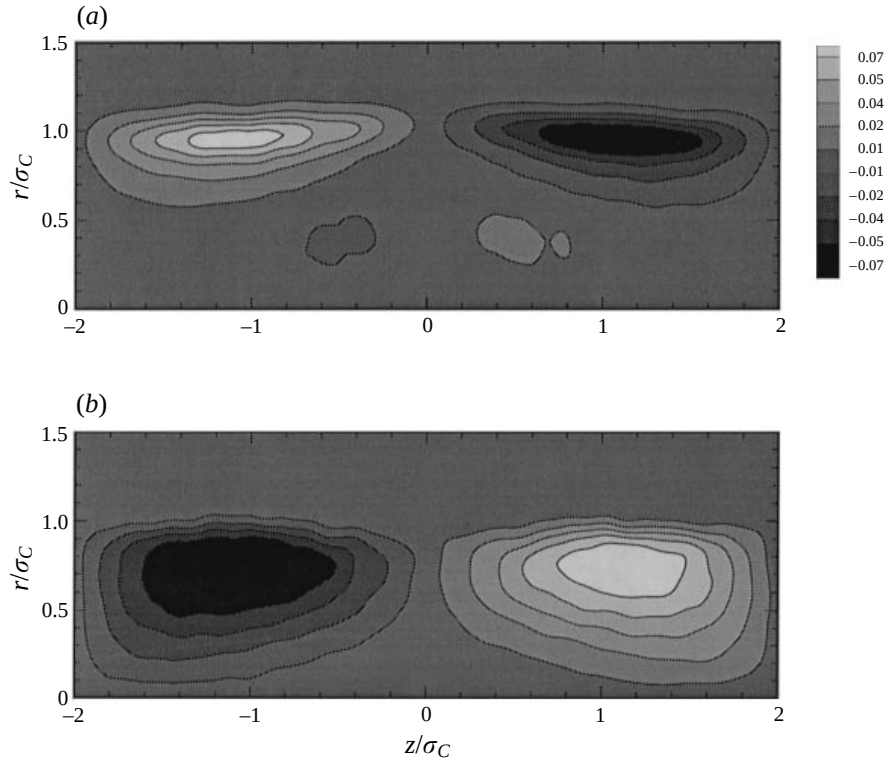

FIGURE 4. Contour plots of the azimuthal vorticity within a standing vortex wave with initial amplitude of 10% of the mean core radius, at dimensionless times (*a*) $t^* = 11.4$ and (*b*) $t^* = 35.4$. The reversal in sign of azimuthal vorticity during the wave period is clearly visible.

$1.12\sigma_C$. The predicted oscillation period (non-dimensionalized by σ_C^2/Γ_C) from (28) using this effective core radius is 39.8. The oscillation period observed in the numerical computation is about 42.3. The preceding results establish the validity of the numerical model to describe the dynamics of the columnar vortex, in the absence of wrapped vortices.

5. The case of identical vortex rings

The computational approaches introduced in §§2 and 3 are now applied to the problem of vortex rings wrapped around a columnar vortex for the case of identical vortex rings. Calculations are first presented based on the approximate model described in §3 in order to explain the qualitative nature of the columnar vortex response to the ring-induced flow. Computations using the vorticity collocation method are then presented to examine the flow field in cases where the approximate model is not adequate.

5.1. *Results from the approximate model*

The system of equations (22) and (23) describing the columnar vortex model can be linearized for small perturbations σ' of the core radius and small axial velocities w to yield the system

$$\frac{\partial \sigma'}{\partial t}+\frac{\sigma_C}{2}\frac{\partial w}{\partial z}=0, \quad \frac{\partial w}{\partial t}+\frac{\Gamma_C^2}{4\pi^2\sigma_C^3}\frac{\partial \sigma'}{\partial z}=0. \tag{29}$$

The forcing term in (23) due to the ring-induced flow, which is independent of time for the case of identical rings (in a frame translating with the rings), is of second order in the axial velocity and hence does not appear in (29). Since the ring-induced axial velocity w_R has a form very similar to a cosine function for the case of identical rings (see figure 5*a*), we consider briefly the idealization

$$w_R(z) = A_1 \cos(2\pi z/L) + A_2, \tag{30}$$

where the constants A_1 and A_2 are obtained by fitting the form (30) to the prediction of (16). The linearized system (29) then yields standing wave solutions for σ' and w of the form

$$\sigma'(z,t) = \frac{\sigma_C A_1}{2c}\sin\left(\frac{2\pi z}{L}\right)\sin\left(\frac{2\pi t}{p}\right), \tag{31a}$$

$$w(z,t) = A_2 + A_1\cos\left(\frac{2\pi z}{L}\right)\cos\left(\frac{2\pi t}{p}\right), \tag{31b}$$

where p is the oscillation period defined by (28).

Results of a computational solution of the nonlinear system (22) and (23) for rings which are much weaker than the columnar vortex ($\Gamma_R/\Gamma_C = 0.2$) are given in figure 5(*a–d*), where the core radius is indicated by a solid curve and the axial velocity by a dashed curve. The initial condition is shown in figure 5(*a*), where the core radius is constant and the axial velocity is equal to the ring-induced velocity w_R plus a constant due to the translation of the rings. The flow evolves initially in a manner similar to that which would be expected from the standing wave solution (31), namely the core radius deforms approximately in the shape of a sine wave and the axial velocity decreases in amplitude and eventually reverses direction, while remaining approximately in the shape of a cosine wave (figure 5*b*). However, as time progresses, the nonlinear forcing

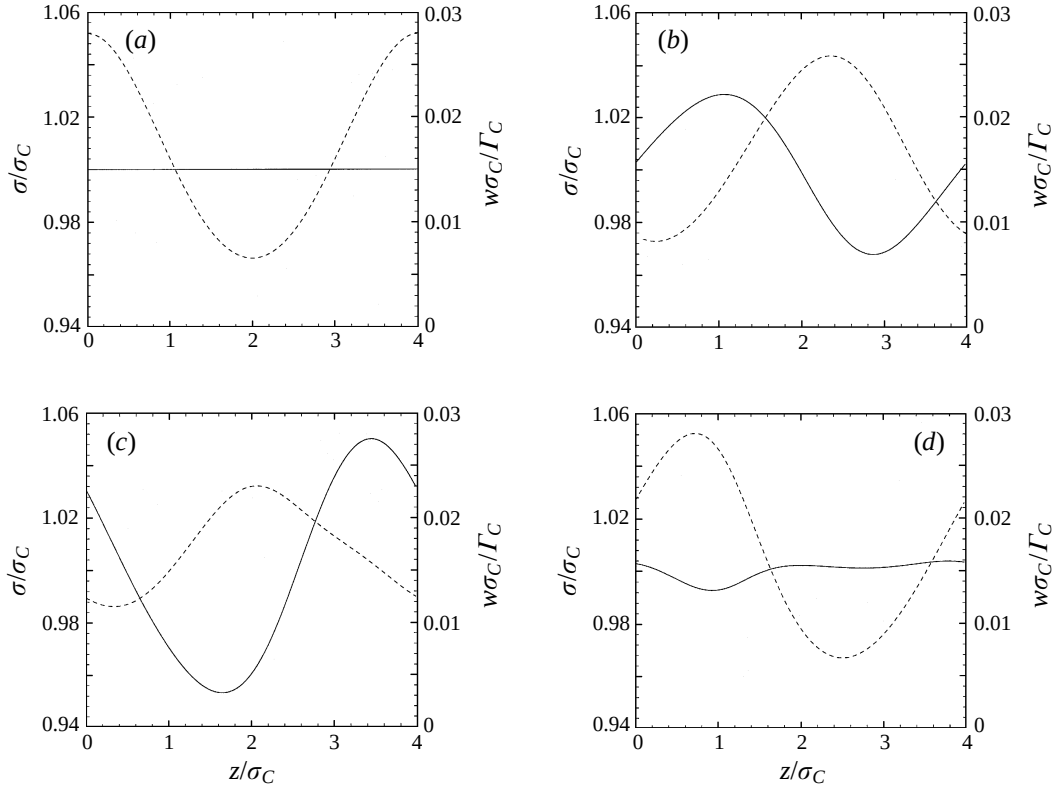

FIGURE 5. Variation of core radius (solid curve) and axial velocity (dashed curve) on the columnar vortex, obtained using the model of §3, for the case of identical vortex rings which are much weaker than the columnar vortex ($\Gamma_R/\Gamma_C = 0.2$). The area-varying waves on the columnar vortex oscillate similar to a standing vortex, but also exhibit a slow upstream propagation relative to the vortex rings, with bounded core radius displacement amplitude of less than 6% of the nominal value, σ_C. Other parameters are $R/\sigma_C = 2$ and $L/\sigma_C = 4$, and the dimensionless times are (*a*) $t^* = 0$, (*b*) $t^* = 14.0$, (*c*) $t^* = 24.0$ and (*d*) $t^* = 36.0$.

term in (23), proportional to $w_R(\partial w_R/\partial z)$, causes the wave in core radius to propagate slowly upstream, as is evident by the offset positions of the wave crest and trough in figure 5(*c*). At the end of one oscillation period p, the core radius is again nearly uniform and the amplitude of the axial velocity variation is nearly the same as in the initial configuration; however, the axial velocity has propagated roughly one-fifth of a wavelength upstream on the vortex axis (figure 5*d*). This sequence of variation of the core radius and axial velocity was followed computationally for over ten periods of oscillation, during which time the slow upstream propagation of the wave continued but the amplitude of oscillation of the core radius never increased above about 6% of the nominal core radius.

Results of a computation for a case with much stronger rings, such that the ring strength is similar to that of the columnar vortex ($\Gamma_R/\Gamma_C = 1$), are given in figure 6(*a–d*). The core radius initially deforms into a sine-wave shape, as for the case with weak vortex rings. However, for cases with strong vortex rings, the amplitude of the axial velocity also becomes large, such that it is possible for the flow on the columnar vortex to exhibit a *critical point* at which the axial flow is equal to the axial wave phase velocity c in (25). For the flow shown in figure 6, the phase speed predicted by (25) is

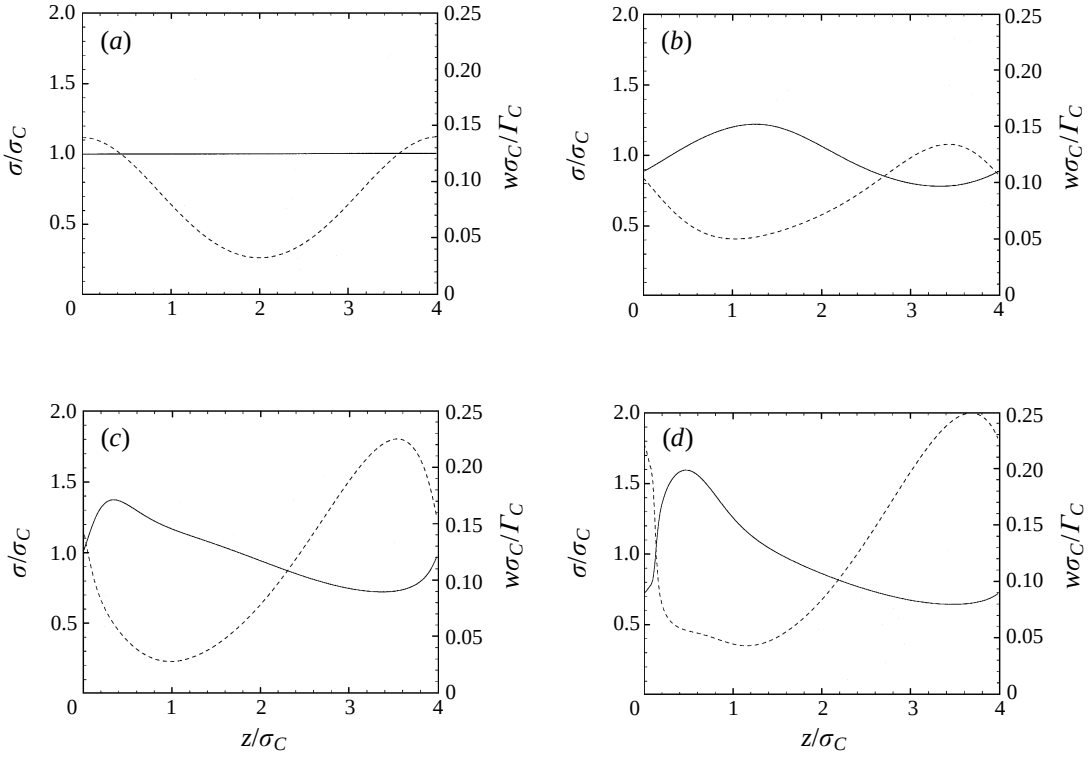

FIGURE 6. Variation of core radius (solid curve) and axial velocity (dashed curve) on the columnar vortex, obtained using the model of §3, for the case of identical vortex rings with strength similar to that of the columnar vortex ($\Gamma_R/\Gamma_C = 1$). Wave energy is trapped on the columnar vortex core downstream of a critical point, such that the wave amplitude continues growing and the wave becomes progressively steeper with time. The dimensionless times are (*a*) $t^* = 0$, (*b*) $t^* = 9.0$, (*c*) $t^* = 17.0$ and (*d*) $t^* = 21.0$.

$c = 0.113$, so that critical points occur in the initial configuration in figure 6(*a*) at z/σ_C equal to 0.6 and 3.4. As the wave propagates upstream due to the nonlinear forcing term, as described in the last paragraph, it is blocked by the transition from subcritical to supercritical flow at the critical flow, leading to a trapping of wave energy just downstream of the critical point. The trapped wave energy manifests itself in the formation of a wave in core radius which grows in amplitude and becomes progressively steeper in time on the subcritical side of the critical point, as shown in figures 6(*c*) and 6(*d*). The core radius variation at the critical point eventually becomes so steep that the numerical method used to solve (22) and (23) yields spurious small-scale squiggles (see the discussion in Peyret & Taylor 1990, p. 49) and must be stopped. We note that a somewhat similar energy trapping mechanism was previously proposed by Randall & Leibovich (1973) as a model for vortex breakdown. Also, Marshall (1993) showed that for a system similar to (22) and (23), with a term due to ambient pressure gradient replacing the ring-induced forcing terms, the amplitude of upstream-propagating waves on the vortex core becomes unbounded at the critical point in the linear theory. This analysis was repeated for the system (22) and (23) for the present problem, yielding the same result.

5.2. *Computational results from the vorticity collocation method*

Computations were performed using the axisymmetric vorticity collocation method described in §2 to examine the columnar and ring vortex interaction when the conditions for validity of the approximate model given in §3 are exceeded. The computations follow the evolution of a single period of the vortex in the axial direction, where a sufficient number of additional periods of the vorticity field on each side of the computed section are used in the Biot–Savart calculation to ensure that the velocity deviates from periodic by no more than 3%. The required number of additional periods was set by the criterion $[(L/R)^2+1]^{-3/2} < 0.03$, which was developed using an error estimate based on the flow generated by a periodic series of vortex rings.

The vorticity within the ring is discretized using 316 ring-like vorticity elements, which are grouped together to form a torus. The columnar vortex is initiated using 2020 ring-like vorticity elements and 101 blob-like elements along the symmetry axis. The vorticity elements in the columnar vortex were initially spaced an equal distance apart, with 21 elements across the core radius at each of $20(L/\sigma_C)+1$ axial locations, and then the control point locations were randomly perturbed by up to 30% of their initial separation distances prior to start of the computations. The vorticity field within the columnar vortex is specified to be initially uniform and oriented in the axial direction. The vorticity within the ring is oriented in the azimuthal direction, and the vorticity magnitude is initially specified to be proportional to the distance r from the symmetry axis. The flow was evolved using an explicit two-step predictor–corrector method. For viscous flow calculations, the time step was set adaptively using the criterion (15) with $s = 2$. For all computations reported here, the flow parameters were set such that $\sigma_C/\sigma_R = 2$ and $R/\sigma_C = 2$, and the equations of motion are inviscid unless otherwise stated.

The first set of calculations examines the stability of the vortex ring cores as the value of the ratio L/σ_R is varied. For very large values of L/σ_R the core shape of the vortex rings remains fairly circular during the calculation, but as this ratio is decreased the core of the rings become progressively more deformed. If L/σ_R is decreased below some critical value, the ring cores become unstable and flatten out. An example illustrating the consequences of the ring core instability is shown in figure 7(*a–d*) for a case with $L/\sigma_R = 4$, $\Gamma_C/\Gamma_R = 1$ and three periods of the vorticity field used on each side of the computed section. The deformation of the ring cores is observed to become progressively more pronounced with time in figure 7(*a–c*), until the cores of neighbouring vortices overlay each other to form a continuous 'sheath' enclosing the columnar vortex (figure 7*d*). The ring core instability occurs sufficiently quickly that only very small wave motions on the columnar vortex are observed.

The instability of the ring cores results from straining on each ring due to the velocity induced by the other rings. Since the vorticity within the centre vortex is predominantly oriented in the axial direction, and therefore has negligible effect on the interaction of the rings with each other, a series of calculations was performed using only the ring vortices in order to determine a criterion for ring core instability. The calculations were performed for a case with $R/\sigma_R = 4$ and for different values of L/σ_R, using 5 periods on each side of the computed ring. The ring cores are found to be unstable (leading to merger of the ring cores into a continuous layer) whenever the ratio L/σ_R is less than 4.8 ± 0.2, and to be stable when L/σ_R is greater than this value. Calculations with a larger number of periods and with different values of R/σ_R indicate that the critical value of L/σ_R is not sensitive to these parameters, although calculations were not performed with very small R/σ_R values. The critical L/σ_R value for vortex core

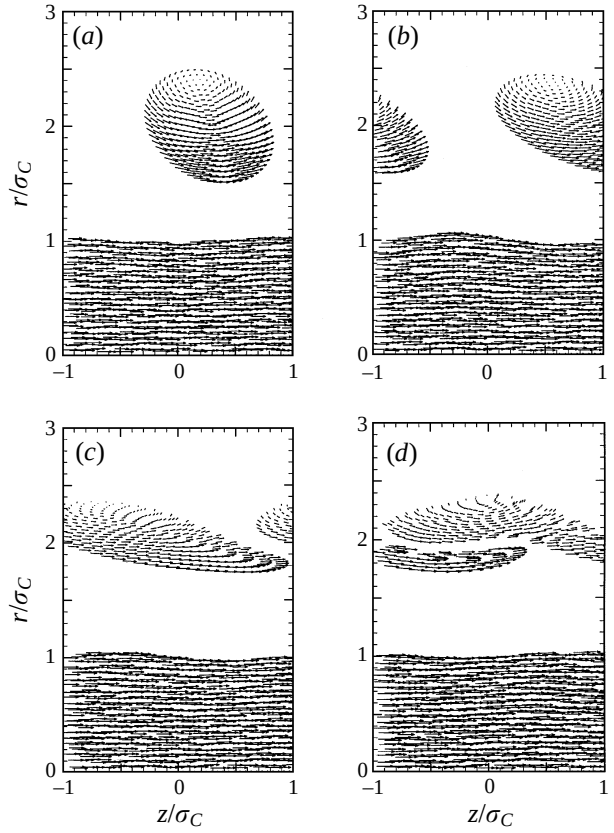

FIGURE 7. Velocity vectors in the (r, z)-plane obtained from direct computation of the ring–columnar vortex interaction, using the vorticity collocation method, for a case with identical rings and small ring spacing ($L/\sigma_R = 4$). The ring cores are unstable and spread out into a 'sheath' surrounding the columnar vortex core. Other parameters are $\Gamma_R/\Gamma_C = 1$, $R/\sigma_C = 2$ and $L/\sigma_C = 2$, and the dimensionless times are (*a*) $t^* = 0.8$, (*b*) $t^* = 2.8$, (*c*) $t^* = 6.8$ and (*d*) $t^* = 9.8$.

instability for an infinite row of initially circular two-dimensional vortex patches of the same strength was obtained as 4.5 by Ferziger (1980) using a theoretical argument, which is quite close to the value obtained numerically in the present study for core instability of vortex rings.

It is possible that the 'sheath' about the columnar vortex formed by the remnants of the ring vortices (figure 7*d*) may eventually roll up to form new ring vortices with a larger value of the period L. Repeated vortex breakup and formation in a two-dimensional shear layer was reported, for instance, by Manin (1992). However, since our primary interest in the current paper is in the columnar vortex response, rather than interaction of the ring vortices, we shall limit consideration in the following to cases where breakup of the ring vortices does not occur.

When the rings are spaced sufficiently far apart that the cores are stable, the ring-induced flow causes the formation of area-varying waves on the vortex core, the amplitude of which increases with increase in the ring strength. We have already described the oscillatory nature of the columnar vortex waves and the slow upstream propagation of these waves due to nonlinear effects for weak vortex rings (using the model described in §3), and we now seek to examine the deviation of the columnar vortex evolution from this behaviour when the ring vortices are fairly strong. To this

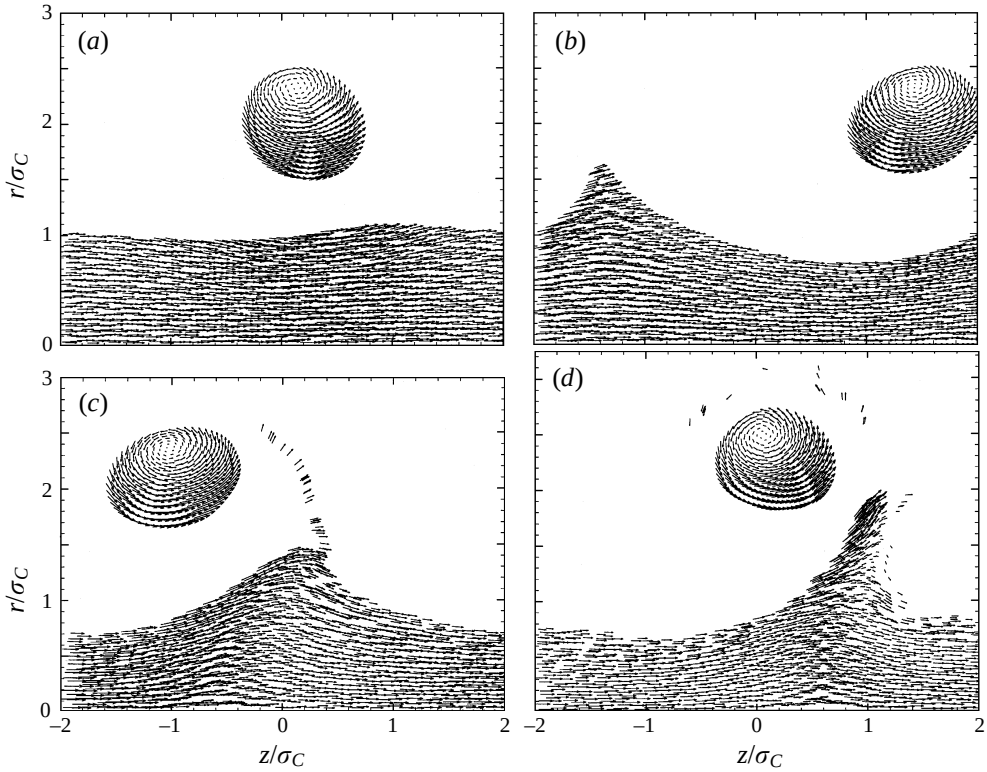

FIGURE 8. Velocity vectors in the (r, z)-plane obtained from direct computation of the ring–columnar vortex interaction, using the vorticity collocation method, for a case with identical rings and $\Gamma_R/\Gamma_C = 1$. A sharp cusp forms at the wave crest, from which vorticity is ejected away from the columnar vortex into the flow. Other parameters are $R/\sigma_C = 2$, $\sigma_C/\sigma_R = 2$ and $L/\sigma_C = 4$, and the flow is inviscid. The dimensionless times are (*a*) $t^* = 0.8$, (*b*) $t^* = 8.8$, (*c*) $t^* = 18.8$ and (*d*) $t^* = 26.8$.

end, the results of a calculation using the vorticity collocation method for strong vortex rings ($\Gamma_R/\Gamma_C = 1$) with spacing given by $L/\sigma_R = 8$ are shown in figure 8(*a–d*) (for the velocity field in the r, z-plane), for a case with two periods of the vorticity field on each side of the computed section. The parameter values used in this calculation are the same as those used to obtain figure 6, which was based on the approximate model of §3, and the flow is inviscid.

In this computation, the ring-induced velocity field is initially observed to cause the formation of a wave in the columnar vortex which travels with the rings, similar to that shown in figure 6(*b*). However, when the amplitude of the wave becomes sufficiently large (at about 50% of the nominal core radius) a sharp cusp is observed to form at the wave crest (figure 8*b*). Vorticity from the columnar vortex is ejected from this cusp in the form of a very thin vortex sheet, which is drawn upward by the rings (figure 8*c*). As the ejected vorticity sheet is drawn out from the columnar vortex, the point of attachment of this sheet with the columnar vortex also moves slowly downstream. A large-amplitude wave in the columnar vortex develops just upstream of the sheet attachment point, resulting eventually in ejection of a large bulk of the columnar vortex (figure 8*d*).

Streamlines in the (r, z)-plane and a contour plot of the azimuthal velocity are given in figures 9(*a*) and 9(*b*) at a time when a vortex sheet has just been ejected from the columnar vortex (corresponding to figure 8*c*). Both of these plots were obtained by

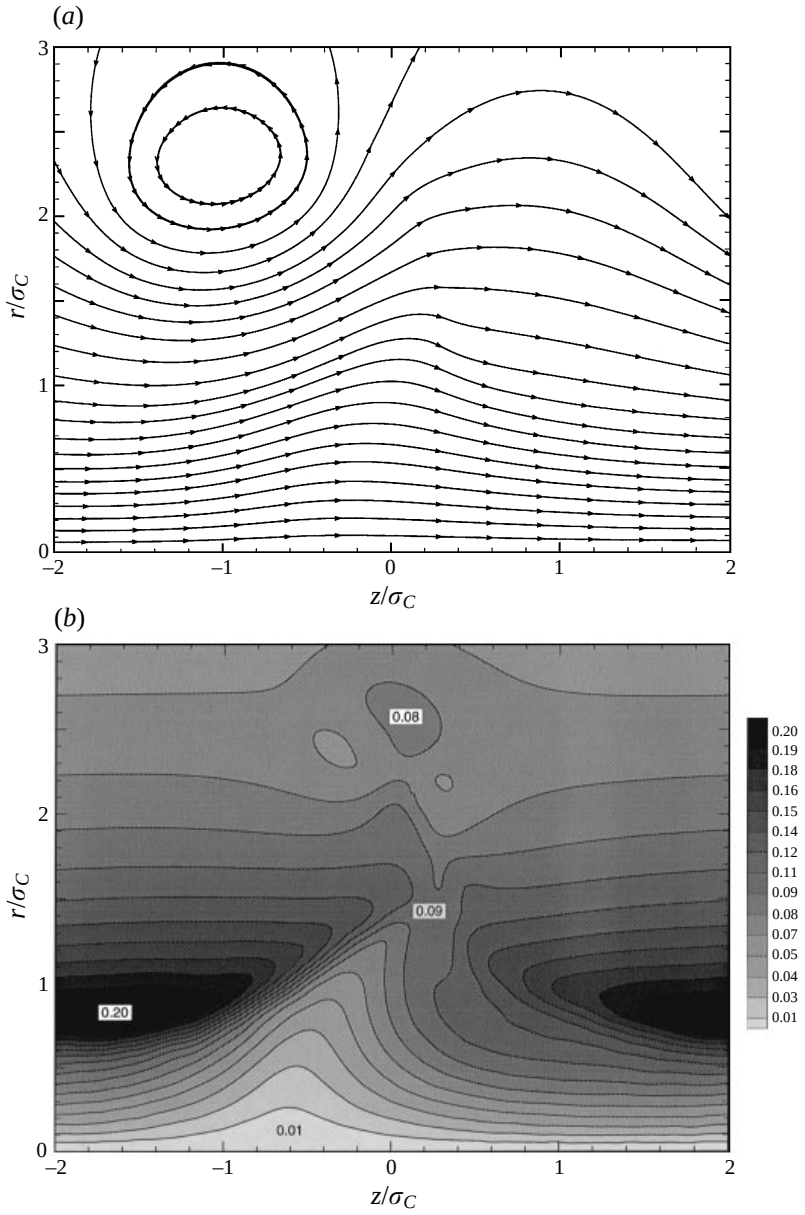

FIGURE 9(*a*, *b*). For caption see facing page.

evaluating the velocity on a 151×201 uniform grid. The streamlines in the (r, z)-plane are dominated by the vortex rings and seem to be relatively unaffected by the ejected vortices. By contrast, the azimuthal velocity in figure 9(*b*) is not significantly affected by the rings, but clearly shows the effect of the large-amplitude wave on the columnar vortex core.

The vorticity vectors in the (r, z)-plane and a contour plot of the azimuthal vorticity are shown in figures 9(*c*) and 9(*d*) at this same time. The ejected vorticity sheet in figure 9(*c*) is two-sided, such that the direction of the vorticity vector is opposite on opposite sides of the sheet. Since the ejected vorticity sheet is stretched by the ring-induced flow,

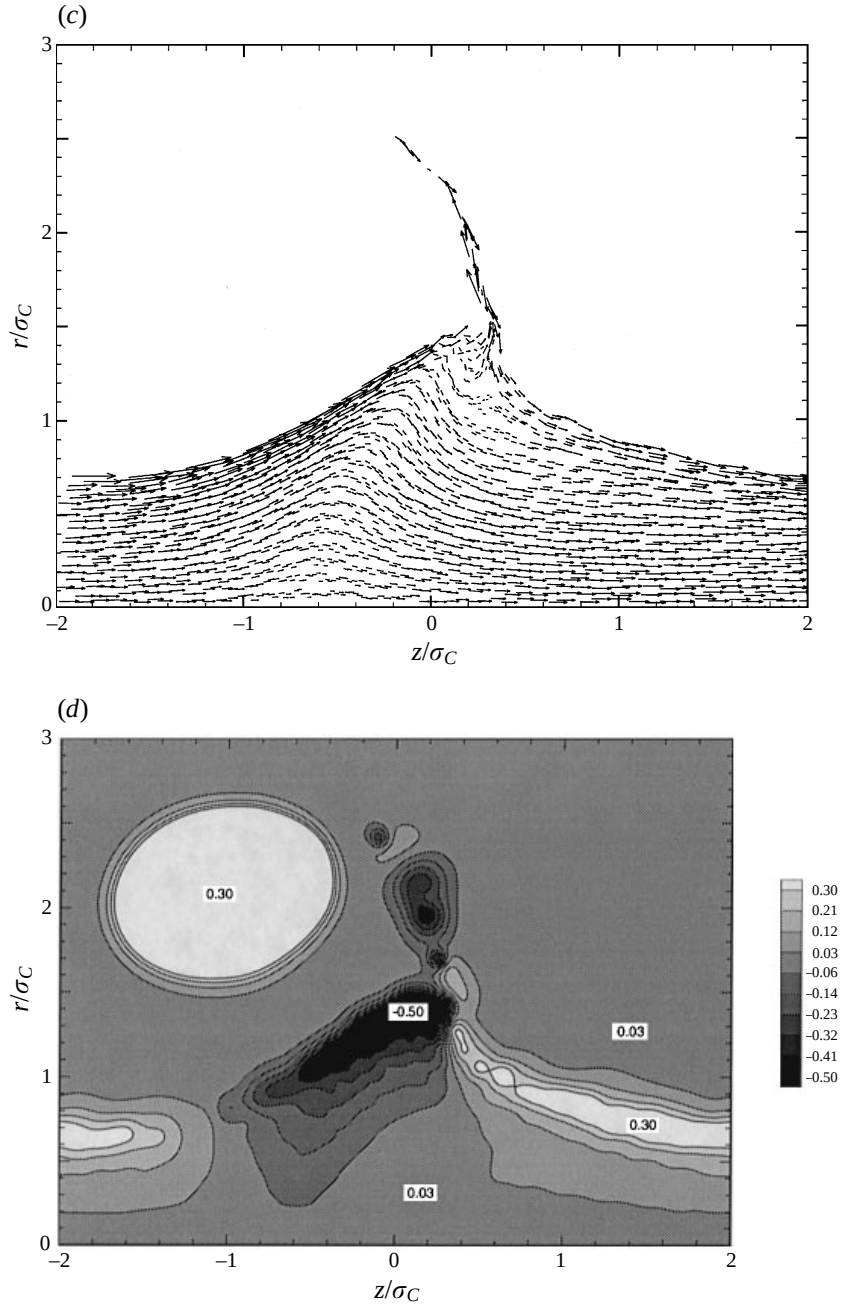

FIGURE 9. Plots examining the ring-induced eruption from an inviscid columnar vortex for the case in figure 8 at dimensionless time $t^* = 18.8$. (*a*) Streamlines in the (r, z)-plane, (*b*) azimuthal velocity contours, (*c*) vorticity vectors in the (r, z)-plane and (*d*) azimuthal vorticity contours.

the vorticity in this sheet can become large after long time for an inviscid flow. The contour plot for the azimuthal vorticity was obtained by interpolating vorticity onto a 151×201 grid in the (r, z)-plane using the representation (4). The ejected sheet appears to be much thicker in the contour plot in figure 9(*d*) than in figure 9(*c*) due to use of the interpolation (4) with finite-radius vorticity elements.

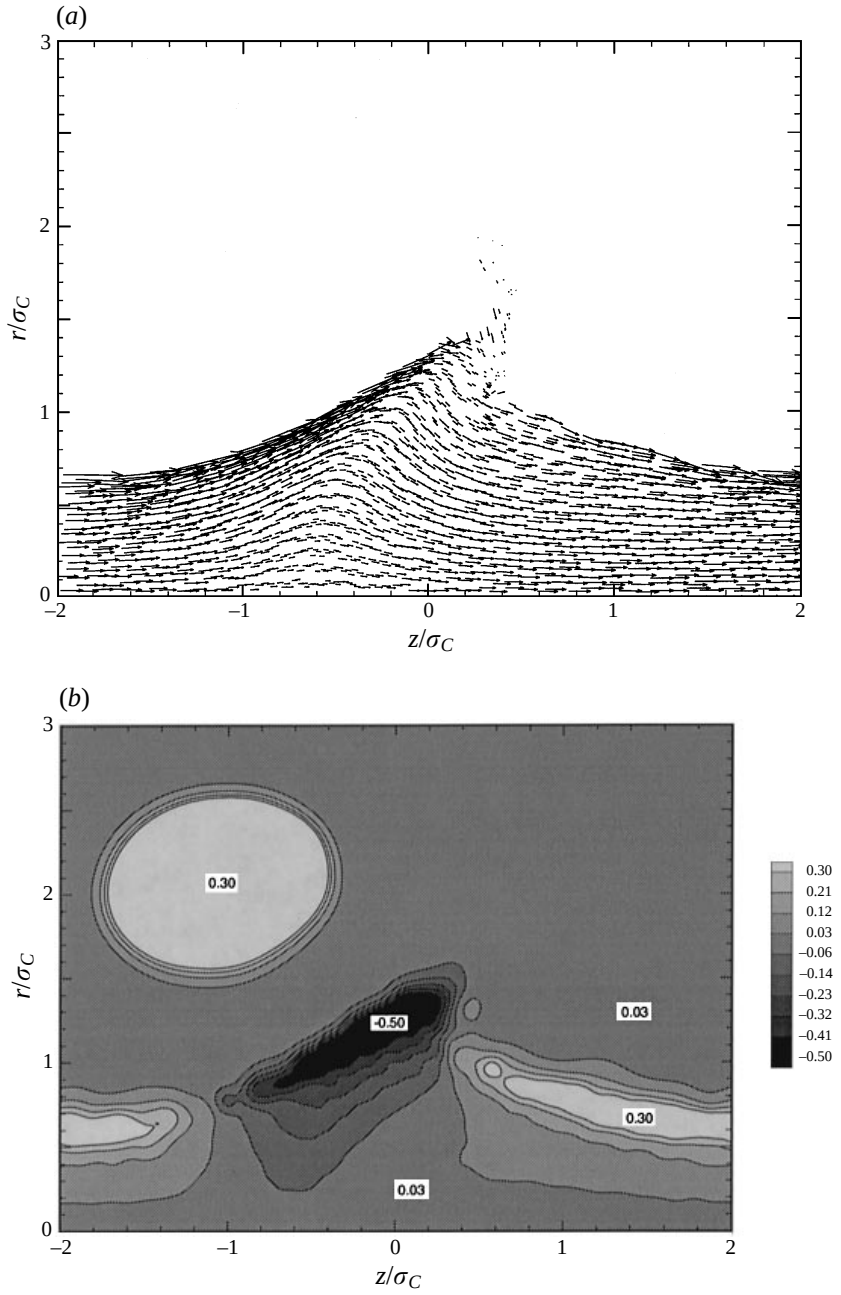

FIGURE 10. Vorticity field for a calculation with the same parameters values and at the same time as in figure 9, except that the flow is viscous, with a vortex Reynolds number $Re = 1000$. The vorticity vectors in the (r, z)-plane are shown in (*a*) and a contour plot of the azimuthal vorticity is shown in (*b*).

This calculation was repeated for viscous flow with several different values of the vortex Reynolds number ($Re \equiv \Gamma_C/\nu$). For instance, the vorticity field is shown in figure 10 for a calculation with the same parameter values and at the same time as in figure 9, but for a viscous flow with $Re = 1000$. The wave formation and subsequent

ejection of vorticity occurs in a similar manner for viscous and inviscid flows, as evidenced by the similarity in the vorticity field within the ring and the columnar vortex in figures 9 and 10. However, for the viscous flow shown in figure 10, the vorticity within the ejected vortex sheet is observed to rapidly diffuse into a thick region with very weak vorticity (such that the ejected vorticity is hardly visible in figure 10), while in the inviscid flow the ejected vorticity remains in a thin sheet and can become quite strong as it is stretched by the ring-induced flow. It is noted that since a Lagrangian computational method is used to obtain these plots, there is almost no numerical dissipation to contaminate the inviscid flow calculation.

6. The case of vortex rings of alternating sign

6.1. *Results from the columnar vortex model*

For the case of rings of alternating sign, the ring-induced axial velocity w_R has a form very similar to a sine function (see figure 11*a*), so we consider the idealization

$$w_R(z) = A_1 \sin(2\pi z/L) + A_2, \tag{32}$$

where the constants A_1 and A_2 are obtained by fitting the form (32) to the prediction of (16). If we assume that the motion of the rings is so small as to be negligible during the wave period p, the linearized system (29) yields standing wave solutions for σ' and w of the form

$$\sigma'(z,t) = \frac{\sigma_C A_1}{2c}\cos\left(\frac{2\pi z}{L}\right)\sin\left(\frac{2\pi t}{p}\right), \tag{33a}$$

$$w(z,t) = A_2 + A_1 \sin\left(\frac{2\pi z}{L}\right)\cos\left(\frac{2\pi t}{p}\right). \tag{33b}$$

Results of a computational solution for the nonlinear system (22) and (23) for the case of fairly weak rings ($\Gamma_R/\Gamma_C = 0.2$) of alternating sign are shown in figure 11(*a–d*). The core radius and axial velocity are observed to oscillate as a standing wave, with no tendency to propagate along the vortex axis (as was observed for the case of identical rings). As time progresses, vortex rings of opposite sign approach each other and propagate radially outward. This causes higher-frequency waves to form in the axial velocity in figure 11(*c*) and a narrowing of the peak in core radius in figure 11(*d*). The core radius is nearly uniform in figure 11(*d*) and the axial velocity has a shape similar to that in the initial configuration, with a somewhat steeper slope near the centre. However, the observed time in figure 11(*d*) is about 50% longer than the predicted period from (28). The maximum deflection of the core radius and the maximum axial velocity on the columnar vortex both increase as the ring strength increases. For instance, results of a calculation with $\Gamma_R/\Gamma_C = 1$ given in figure 12(*a*, *b*) show that the peak in core radius can become quite large compared to the minimum core radius.

6.2. *Computational results from the vorticity collocation method*

Calculations based on the vorticity collocation method are used to examine the possibility of entrainment of vorticity from the columnar vortex by the rings as the wave amplitude on the columnar vortex becomes large. Because two rings are contained within each period of the flow for cases with rings of alternating sign, L/R is sufficiently large that we need include only one period of the vorticity field on each side of the computed section to achieve the desired accuracy in the computations in

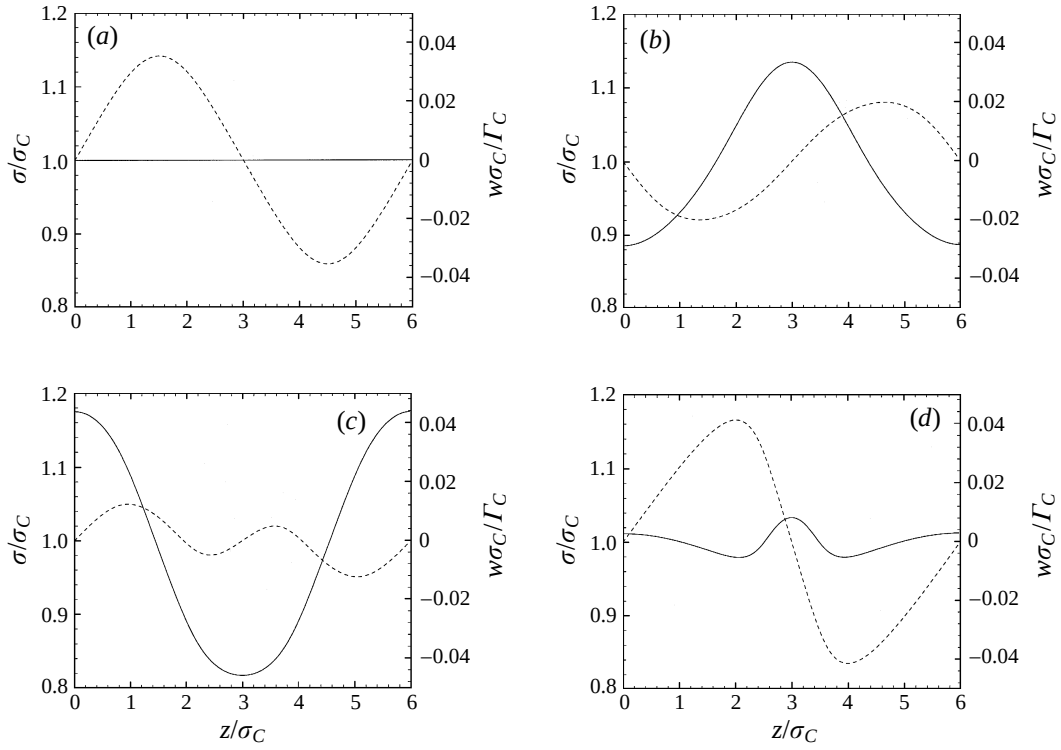

FIGURE 11. Variation of core radius (solid curve) and axial velocity (dashed curve) on the columnar vortex, obtained using the model of §3, for the case of vortex rings with alternating sign. The rings are much weaker than the columnar vortex ($\Gamma_R/\Gamma_C = 0.2$), and area-varying waves on the columnar vortex oscillate as standing waves on the vortex core. The waves are not periodic, but exhibit a peak which grows gradually narrower with time due to the motion of the vortex ring pair which forces the flow. Other parameters are $R/\sigma_C = 2$ and $L/\sigma_C = 6$, and the dimensionless times are (*a*) $t^* = 0$, (*b*) $t^* = 18.0$, (*c*) $t^* = 42.0$ and (*d*) $t^* = 54.0$.

this section. An initial calculation was performed for the case of fairly weak rings ($\Gamma_R/\Gamma_C = 0.2$), for a viscous flow with $Re = 1000$ and with one period on each side of the computed section. The parameter values for this computation are the same as those used to generate figure 11. The velocity field at three different time steps is shown in figure 13(*a–c*). Just after the flow is started (figure 13*a*), the ring-induced velocity causes the formation of a wave on the columnar vortex. The amplitude of this wave is similar to that predicted by the approximate model of §3, as can be seen by comparing figure 13(*b*) and figure 11(*b*), which are plotted at approximately the same times. The displacement of the core radius causes the generation of azimuthal vorticity on the columnar vortex, which resists the wave formation and eventually causes the wave to recede (figure 13*c*). However, we do observe that a small amount of vorticity from the columnar vortex is entrained into the rings in figure 13(*c*).

Results of a calculation with much stronger vortex rings ($\Gamma_R/\Gamma_C = 1$) are shown in figure 14(*a–d*) for the velocity components in the (r, z)-plane, for a viscous flow with $Re = 1000$. The parameters for this calculation are the same as those used to generate figure 12, which was obtained using the model of §3. In the direct calculations with the vorticity collocation method, the ring-induced flow is observed to induce a large-amplitude wave on the columnar vortex, which appears similar to that predicted in figure 12(*b*). Although azimuthal vorticity is generated on the columnar vortex core,

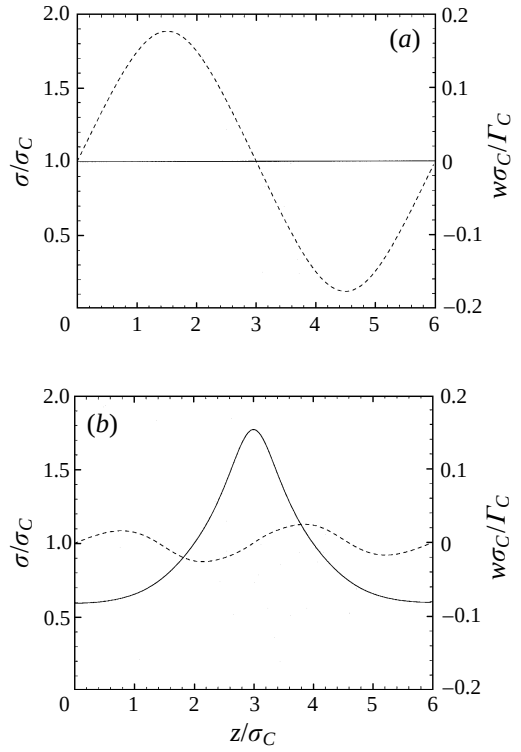

FIGURE 12. Variation of core radius (solid curve) and axial velocity (dashed curve) on the columnar vortex, obtained using the model of §3, for the case of vortex rings with alternating sign. The rings have a strength similar to that of the columnar vortex ($\Gamma_R/\Gamma_C = 1$), and the columnar vortex responds to the ring-induced velocity by formation of a large-amplitude peak in the core radius. Other parameters are $R/\sigma_C = 2$ and $L/\sigma_C = 6$, and the dimensionless times are (*a*) $t^* = 0$ and (*b*) $t^* = 10.0$.

it is insufficient to counter the ring-induced flow. The wave amplitude is thus observed to continue growing in time, leading to an ejection of vorticity from the columnar vortex in the form of a two-sided sheet. This sheet is initially much thicker in the present case of rings of alternating sign than was observed for identical rings in §5, and the ejected vorticity is consequently much less effected by viscous diffusion. As the rings propagate radially outward, away from the columnar vortex, the magnitude of the ring-induced velocity decreases near the columnar vortex. After the rings propagate a sufficient distance away, the flow induced by the azimuthal vorticity within the columnar vortex is able to dominate the ring-induced flow, thus allowing the wave in vortex core radius to decrease in amplitude (figure 14*d*). As the ejected vorticity is pulled radially outward by the vortex rings and the wave on the columnar vortex begins to recede, the ejected vorticity is rapidly stretched in the radial direction. This stretching causes the ejected vortex sheet to become very thin and to dissipate rapidly.

Streamlines in the (r, z)-plane and a contour plot of the azimuthal velocity are shown in figures 15(*a*) and 15(*b*) for a time corresponding to that in figure 14(*c*). Both plots were obtained by evaluating the velocity on a 301×201 uniform grid. The streamlines in the (r, z)-plane show both the rotation induced by the vortex ring pair and that induced by the azimuthal vorticity within the columnar vortex. The azimuthal velocity shows a strong decrease where the vorticity from the columnar vortex has been pulled outward by the rings.

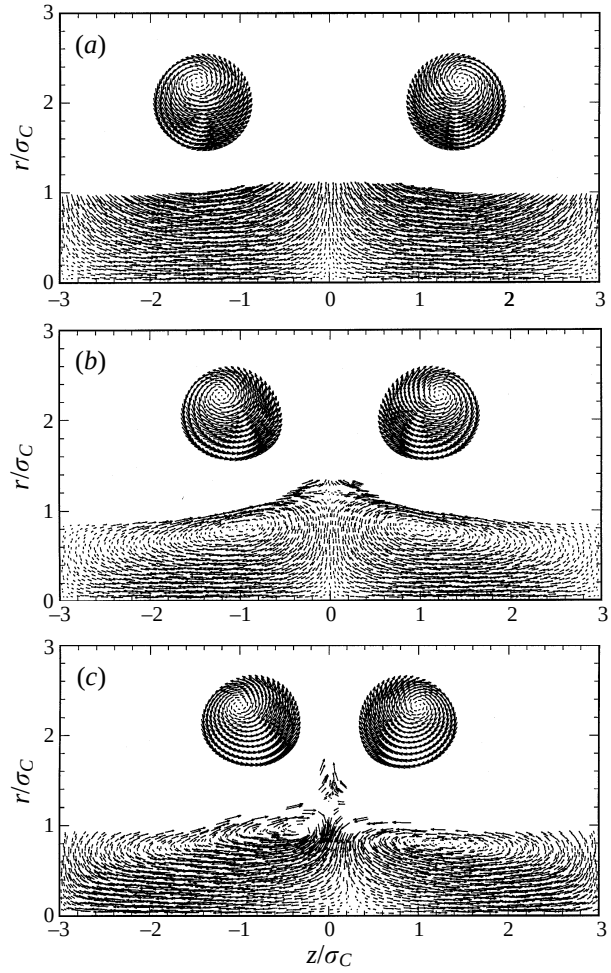

FIGURE 13. Velocity vectors in the (r, z)-plane obtained from direct computation of the ring–columnar vortex interaction, using the vorticity collocation method, for a case with fairly weak rings ($\Gamma_R/\Gamma_C = 0.2$) of alternating sign. A wave on the columnar vortex forms due to the ring-induced flow, which then subsides due to the azimuthal vorticity field generated by the core radius variation. The response of the columnar vortex to the ring-induced flow is primarily to generate a standing wave, although a small amount of vorticity from the columnar vortex is entrained by the ring pair. Other parameters are $R/\sigma_C = 2$, $\sigma_C/\sigma_R = 2$, and $L/\sigma_C = 6$. The flow is viscous with $Re = 1000$. The dimensionless times are (*a*) $t^* = 1.6$ (*b*) $t^* = 18.4$ and (*c*) $t^* = 31.1$.

The vorticity vectors in the (r, z)-plane and a contour plot of the azimuthal vorticity are shown in figures 15(*c*) and 15(*d*) for the same time as in figure 14(*c*) and again in figures 16(*a*) and 16(*b*) for the later time used in figure 14(*d*). The vorticity vectors within the ejected vortex sheet are in opposite directions on opposite sides of the sheet (figures 15*c* and 16*a*). As the vorticity sheet becomes very stretched out by the ring-induced flow, the number of vorticity control points across the sheet reduces to only a few. Because of the high shear across the sheet, the vorticity vectors at the control points become subject to a numerical instability as the resolution deteriorates in which a slight wobble in the vector direction leads to large stretching of the vorticity. This stretching is countered by rapid diffusion of the vorticity sheet, which limits the magnitude of the vorticity vectors and hence does not lead to global breakdown of the

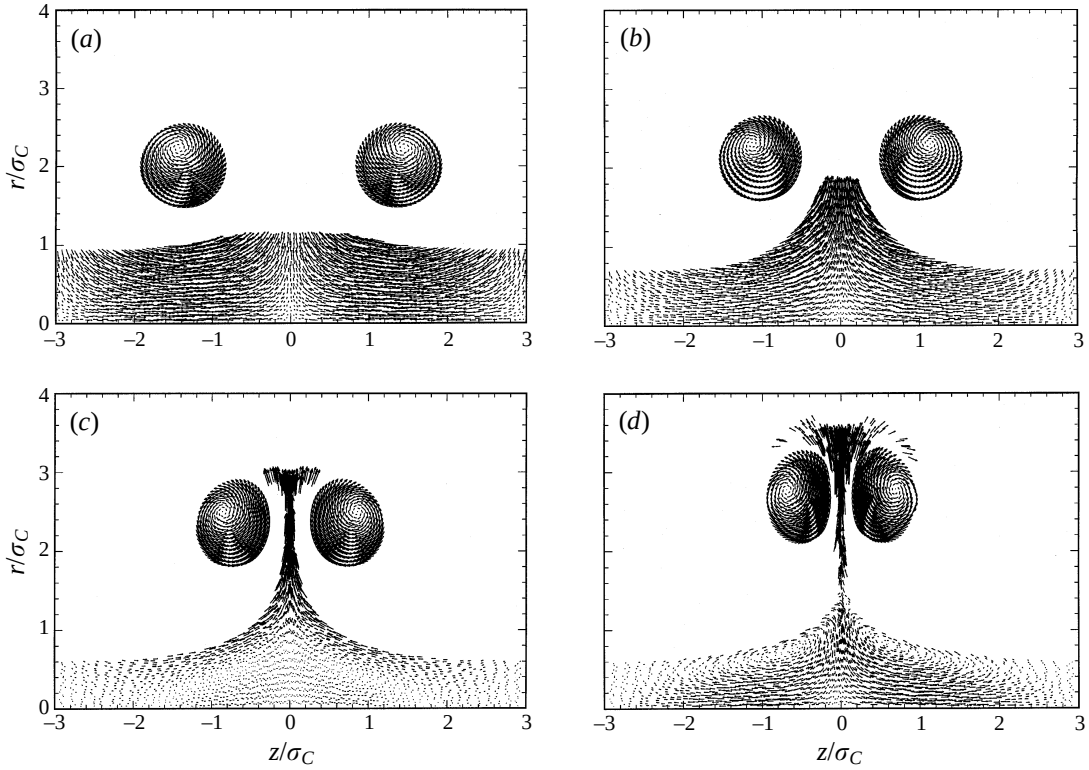

FIGURE 14. Velocity vectors in the (r, z)-plane obtained from direct computation of the ring–columnar vortex interaction, using the vorticity collocation method, for a case with fairly strong rings ($\Gamma_R/\Gamma_C = 1$) of alternating sign. Vorticity from the columnar vortex is entrained by the pair of oppositely signed vortex rings, leaving a thin two-sided sheet of vorticity trailing behind. Other parameters are $R/\sigma_C = 2$, $\sigma_C/\sigma_R = 2$, and $L/\sigma_C = 6$. The flow is viscous with $Re = 1000$. The dimensionless times are (*a*) $t^* = 0.7$ (*b*) $t^* = 5.2$, (*c*) $t^* = 9.6$ and (*d*) $t^* = 13.1$.

calculation. At long time (e.g. figures 16*a* and 16*b*), the ejected vorticity dissipates away nearly completely and the ring evolution is similar to that depicted in the numerical simulations of colliding axisymmetric rings by Shariff *et al.* (1988).

7. Conclusions

The response of a columnar vortex to periodic stretching and compression induced by vortex rings wrapped around the columnar vortex core is studied using both an approximate model of the columnar vortex dynamics and by numerical solution of the Euler and Navier–Stokes equations in the vorticity–velocity formulation. The ring-induced flow leads to area-varying wave formation on the columnar vortex core. The wave growth on the columnar vortex is resisted by the accumulation of azimuthal vorticity, which is generated due to variation in the core radius. Similarly, in the context of a momentum balance for the columnar vortex core (as used in the Lundgren–Ashurst 1989 model employed in §3), the variation in core radius causes an axial variation in mean pressure across the core, leading to an axial force that resists the core area variation. For sufficiently weak ring vortices, the forcing due to the rings and the restoring motions of the columnar vortex core combine to produce an oscillatory growth and decay of the wave amplitude, where the maximum wave

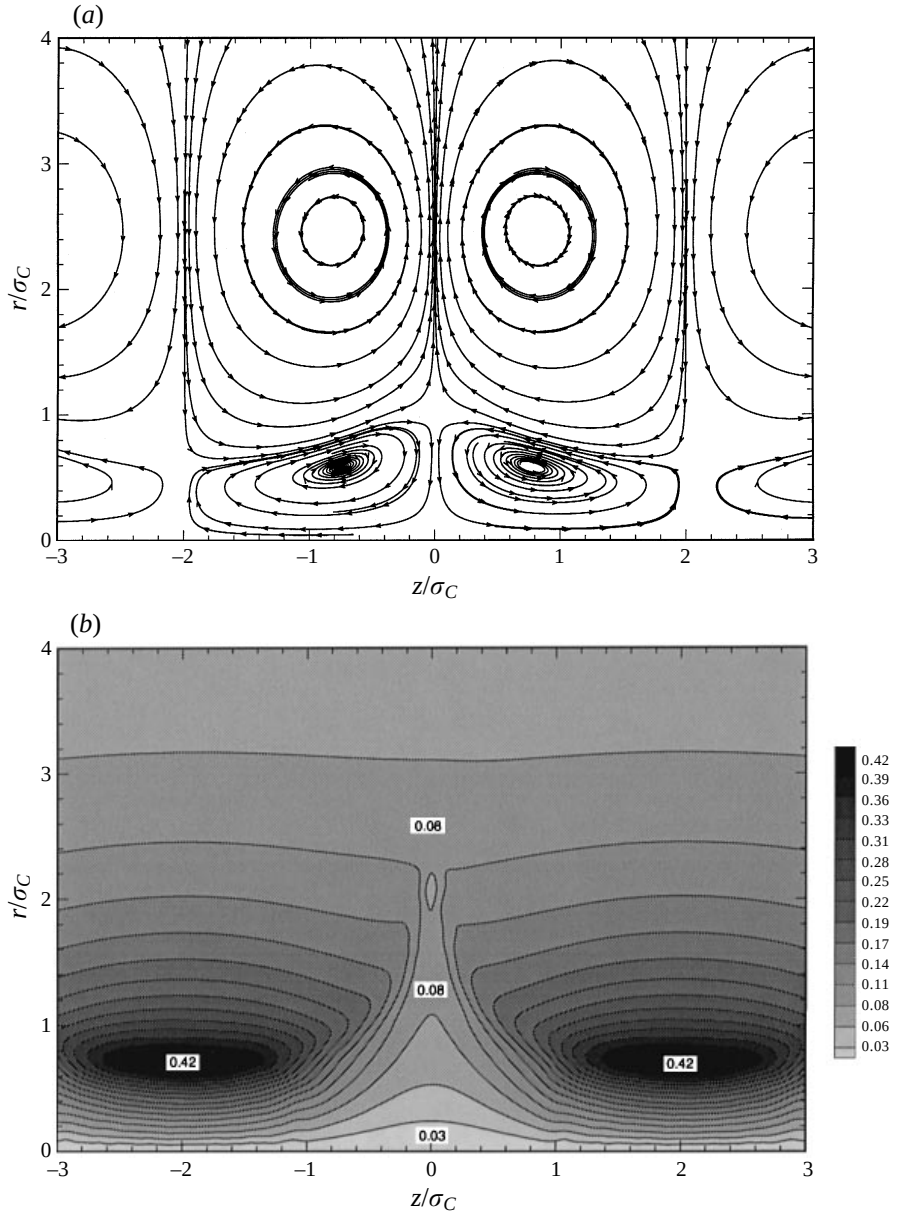

FIGURE 15(*a*, *b*). For caption see facing page.

amplitude is bounded in time. When the rings are sufficiently strong, vorticity from the columnar vortex will be ejected radially outward from the wave crests. This ejected vorticity will be carried away from the columnar vortex by the rings in the form of a double-sided vorticity sheet (where the vorticity points in opposite directions on opposing sides of the sheet). The ejected vorticity is rapidly stretched and (for a viscous fluid) dissipated by the ring-induced flow.

The formation of vortices wrapped around a columnar vortex core is certainly a common occurrence in many turbulent flows, as noted in numerous experimental and direct and large-eddy simulation studies (e.g. Bernal & Roshko 1986; Glezer & Coles

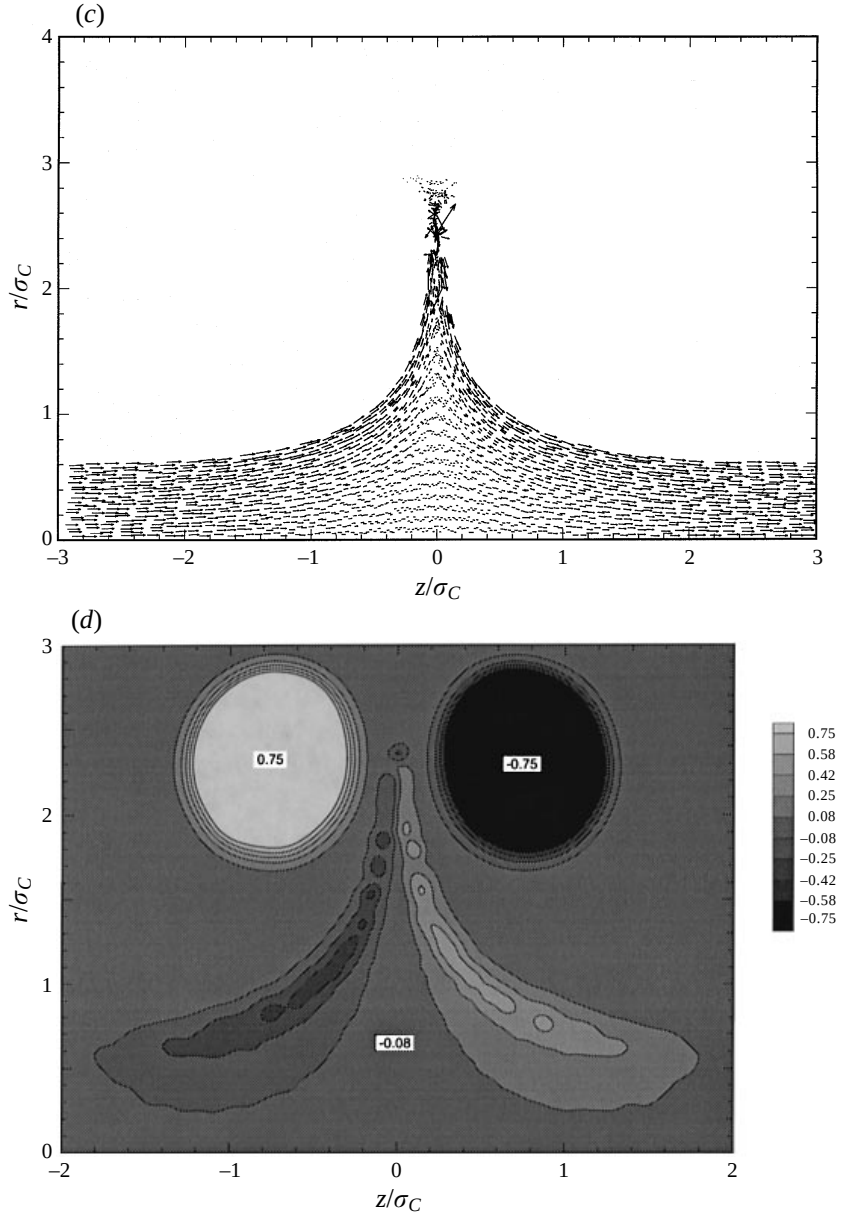

FIGURE 15. Plots examining the ring-induced eruption from an inviscid columnar vortex for the case in figure 14 at dimensionless time $t^* = 9.6$. (*a*) Streamlines in the (r, z)-plane, (*b*) azimuthal velocity contours, (*c*) vorticity vectors in the (r, z)-plane and (*d*) azimuthal vorticity contours.

1990; Lesieur 1995; Melander & Hussain 1993; Sreedhar & Ragib 1994), and is perhaps the most important type of interaction between turbulent eddies of significantly different strengths. The process of ejection of vorticity from the columnar vortex and subsequent rapid diffusion as the ejected vorticity is stretched by the rings, as illustrated by the numerical computations reported in this paper, suggests an interesting mechanism for energy cascade in turbulent flows. In the proposed cascade process, the wrapped vorticity (i.e. the rings) acts somewhat like a catalyst, since the ejected vorticity does not change the structure of the rings, but rather passes directly from the

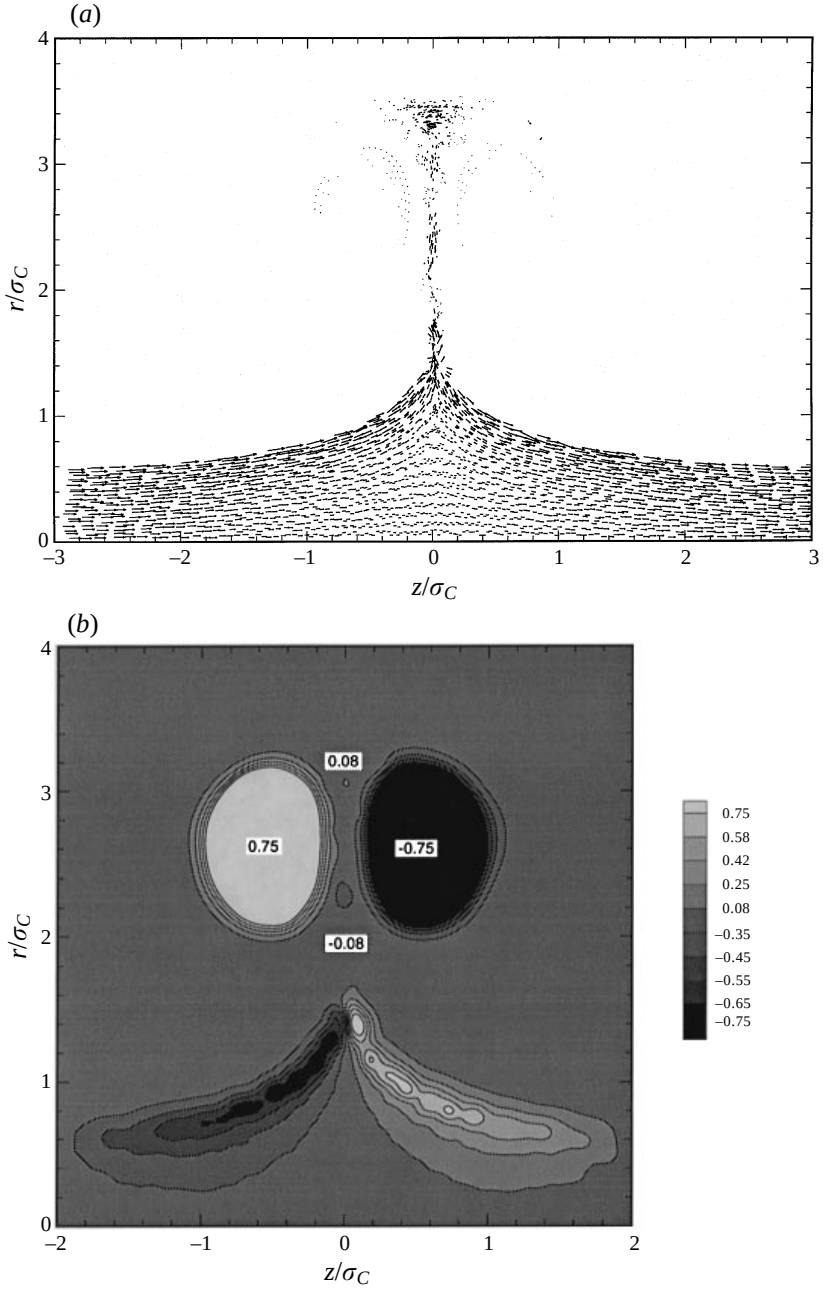

FIGURE 16. Vorticity field for the case in figure 14 at time $t^* = 13.1$. The vorticity vectors in the (r, z)-plane are shown in (*a*) and a contour plot of the azimuthal vorticity is shown in (*b*). Stretching by the rings has made the ejected vorticity layer very thin, leading to rapid dissipation of the ejected vorticity.

larger scale of the columnar vortex to the smaller scale of the double-sided ejected vortex sheet. While rings of alternating sign propagate toward each other and radially outward from the columnar vortex in the axisymmetric simulations shown in the present paper, three-dimensional instability of opposite sign rings (Lim & Nickels 1992) and subsequent vortex wrapping around the columnar vortex may make possible

a state in which statistical measures of the vortex rings are steady. It is noted that even for Reynolds numbers for which the dissipation of the columnar vortex is completely negligible, the ejected vorticity can dissipate quite rapidly as it is stretched by the rings. Dritschel & Zabusky (1996) argue in a recent paper that a similar process in two-dimensional flows, in which a pair of opposite-sign vortex patches cause a third vortex patch to elongate into a thin sheet-like shape, plays a critical role in the cascade process in two-dimensional turbulence.

Research support was provided by the US Army Research Office under Grant number DAAH04-96-0081, Dr Thomas L. Doligalski program manager, with The University of Iowa. Computer time was provided by a grant from the San Diego Supercomputing Center.

REFERENCES

Abramowitz, M. & Stegun, I. A. 1965 *Handbook of Mathematical Functions*. Dover.

Acton, E. 1980 A modelling of large eddies in an axisymmetric jet. *J. Fluid Mech.* **98**, 1–31.

Bernal, L. P. & Roshko, A. 1986 Streamwise vortex structure in plane mixing layers. *J. Fluid Mech.* **170**, 499–525.

Crow, S. C. 1970 Stability theory for a pair of trailing vortices. *AIAA J.* **8**, 2172–2179.

Dritschel, D. G. & Waugh, D. W. 1992 Quantification of the inelastic interaction of unequal vortices in two-dimensional vortex dynamics. *Phys. Fluids* A **4**, 1737–1744.

Dritschel, D. G. & Zabusky, N. J. 1996 On the nature of vortex interactions and models in unforced nearly-inviscid two-dimensional turbulence. *Phys. Fluids* **8**, 1252–1256.

Ferziger, J. H. 1980 Energetics of vortex rollup and pairing. *Phys. Fluids* **23**, 1–4.

Glezer, A. & Coles, D. 1990 An experimental study of a turbulent vortex ring. *J. Fluid Mech.* **211**, 243–283.

Kelvin, Lord 1867 The translatory velocity of a circular vortex ring. *Phil. Mag.* **33**, 511–512.

Kempka, S. N. & Strickland, J. H. 1993 A method to simulate viscous diffusion of vorticity by convective transport of vortices at a non-solenoidal velocity. *Sandia Natl Lab. Tech. Rep.* SAND93-1763.

Kim, J. M. & Komerath, N. M. 1995 Summary of the interaction of a rotor wake with a circular cylinder. *AIAA J.* **33**, 470–478.

Krishnamoorthy, S. & Marshall, J. S. 1997 Three-dimensional vortex-body interaction in a viscous fluid. *ASME Fluids Engineering Division Summer Meeting*, *Vancouver*, *June 22–26*, FED SM 97-3313.

Leonard, A. 1994 Nonlocal theory of area-varying waves on axisymmetric vortex tubes. *Phys. Fluids* **6**, 765–777.

Lesieur, M. R. 1995 Mixing layer vortices. In *Fluid Vortices* (ed. S. I. Green), pp. 35–63. Kluwer.

Levy, H. & Forsdyke, A. G. 1927 The stability of an infinite system of circular vortices. *Proc. Soc. Lond.* A **114**, 594–604.

Lim, T. T. & Nickels, T. B. 1992 Instability and reconnection in the head-on collision of two vortex rings. *Nature* **357**, 225–227.

Liu, H.-T. 1992 Effects of ambient turbulence on the decay of a trailing vortex wake. *J. Aircraft* **29**, 255–263.

Lundgren, T. S. & Ashurst, W. T. 1989 Area-varying waves on curved vortex tubes with application to vortex breakdown. *J. Fluid Mech.* **200**, 283–307.

Manin, D. Yu. 1992 A study of repeated vortex mergers in a forced quasi-2-D shear flow. *Phys. Fluids* A **4**, 1715–1723.

Marshall, J. S. 1991 A general theory of curved vortices with circular cross-section and variable core area. *J. Fluid Mech.* **229**, 311–338.

Marshall, J. S. 1993 The effect of axial pressure gradient on axisymmetrical and helical vortex waves. *Phys. Fluids* A **5**, 588–599.

Marshall, J. S. & Grant, J. R. 1995 A Lagrangian collocation method for vorticity transport in viscous fluid flows. *Proc. Forum on the Application of Vortex Methods to Engineering Problems, Albuquerque, New Mexico, Feb. 22–24.*

Marshall, J. S. & Grant, J. R. 1996 Penetration of a blade into a vortex core: vorticity response and unsteady blade forces. *J. Fluid Mech.* **306**, 83–109.

Marshall, J. S. & Grant, J. R. 1997 A Lagrangian vortex method for viscous, axisymmetric flows with and without swirl. *J. Comput. Phys.* (submitted).

Melander, M. V. & Hussain, F. 1993 Polarized vorticity dynamics on a vortex column. *Phys. Fluids* A **5**, 1992–2003.

Melander, M. V., Zabusky, N. J. & McWilliams, J. C. 1988 Symmetric vortex merger in two dimensions: causes and conditions. *J. Fluid Mech.* **195**, 303–340.

Mittal, R. & Balachandar, S. 1995 Generation of streamwise vortical structures in bluff body wakes. *Phys. Rev. Lett.* **75**, 1300–1303.

Norbury, J. 1973 A family of steady vortex rings. *J. Fluid Mech.* **57**, 417–431.

Ogami, Y. & Akamatsu, T. 1991 Viscous flow simulation using the discrete vortex model – the diffusion velocity method. *Computer Fluids* **19**, 433–441.

Peyret, R. & Taylor, T. D. 1990 *Computational Methods for Fluid Flow*. Springer.

Pierrehumbert, R. T. & Widnall, S. E. 1982 The two- and three-dimensional instabilities of a spatially periodic shear layer. *J. Fluid Mech.* **114**, 59–82.

Randall, J. D. & Leibovich, S. 1973 The critical state: a trapped wave model of vortex breakdown. *J. Fluid Mech.* **58**, 495–515.

Robinson, A. C. & Saffman, P. G. 1982 Three-dimensional stability of vortex arrays. *J. Fluid Mech.* **125**, 411–427.

Saffman, P. G. 1970 The velocity of viscous vortex rings. *Stud. Appl. Maths* **49**, 371–380.

Sarpkaya, T. 1996 Vortices, free surfaces and surfactants. *Ann. Rev. Fluid Mech.* **28**, 83–128.

Shariff, K., Leonard, A., Zabusky, N. J. & Ferziger, J. H. 1988 Acoustics and dynamics of coaxial interacting vortex rings. *Fluid Dyn. Res.* **3**, 337–343.

Sheridan, P. F. & Smith, R. P. 1980 Interactional aerodynamics – A new challenge to helicopter technology. *J. Am. Helicopter Soc.* **25**, 3–21.

Sreedhar, M. K. & Ragib, S. A. 1994 Large eddy simulation of longitudinal stationary vortices. *Phys. Fluids* **6**, 2501–2514.

Strickland, J. H. & Amos, D. E. 1992 Fast solver for systems of axisymmetric ring vortices. *AIAA J.* **30**, 737–746.

Waugh, D. W. 1992 The efficiency of symmetric vortex merger. *Phys. Fluids* A **4**, 1745–1758.